Check for updates

Water Resources Research

RESEARCH ARTICLE
10.1029/2023WR036319

Coupled Hydrogeophysical Modeling to Constrain Unsaturated Soil Parameters for a Slow-Moving Landslide

J. P. Boyd[1,2], J. E. Chambers[1], P. B. Wilkinson[1], P. I. Meldrum[1], E. Bruce[1], and A. Binley[2]

[1]British Geological Survey, Nottingham, UK, [2]Lancaster University, Lancaster, UK

Key Points:

- Geoelectrical methods are useful for investigating moisture content levels inside of unstable slopes
- Unsaturated hydrological modeling parameters can be calibrated with coupled hydrogeophysical modeling
- Calibrated hydrological models indicate the studied landslide retained high moisture contents prior to recorded failures

Supporting Information:

Supporting Information may be found in the online version of this article.

Correspondence to:

J. P. Boyd,
jamyd91@bgs.ac.uk

Citation:

Boyd, J. P., Chambers, J. E., Wilkinson, P. B., Meldrum, P. I., Bruce, E., & Binley, A. (2024). Coupled hydrogeophysical modeling to constrain unsaturated soil parameters for a slow-moving landslide. *Water Resources Research*, *60*, e2023WR036319. https://doi.org/10.1029/2023WR036319

Received 22 SEP 2023
Accepted 9 AUG 2024

Abstract Geophysical methods have proven to be useful for investigating unstable slopes as they are both non-invasive and sensitive to the spatial distribution of physical properties in the subsurface. Of particular interest are the links between electrical resistivity and near-surface moisture content; recent work has demonstrated that it is possible to calibrate hydrological models using geophysical measurements. In this study we explore the use of in-field electrical resistivity data for calibrating unsaturated soil retention parameters and saturated hydraulic conductivity used for modeling unsaturated fluid flow. We study a synthetic case study, and a well-characterized site in the northeast of England and develop an approach to calibrate retention parameters for a mudstone and a sandstone formation, the former being an actively failing unit. Petrophysical relationships between electrical resistivity and moisture content (or saturation) are established for both formations. 2D hydrological models are driven by effective rainfall estimations; subsequently these models are coupled with a geophysical forward model via a Markov chain Monte Carlo approach. For the synthetic case, we show that our modeling approach is sensitive to the moisture retention parameters, while less so to saturated hydraulic conductivity. We observe the same characteristics and sensitivities for the field case, albeit with a greater data misfit. Further hydrological simulations suggest that the slope retained high moisture contents in the months preceding a rotational failure. Therefore, we propose that coupled hydrological and geophysical modeling approaches could aid in enhancing landslide monitoring, modeling, and early warning efforts.

Plain Language Summary The electrical properties of the ground can be particularly useful in characterizing and monitoring landslides, as they are dependent on key physical properties including moisture content, soil/rock composition and porosity (voids). First, different rock types in landslides have different resistivity values, which helps map weak geology at depth. Second, as moisture content in the ground increases it becomes less electrically resistive; this means that the resistivity of the ground changes with the addition of water, usually from rainfall. In this research, we use the relationships between electrical resistivity and soil moisture to calibrate models of fluid flow in the subsurface for a known landslide. The issue with unstable slopes is that failure is often associated with increased moisture content, therefore modeling fluid flow in the subsurface is important for assessing slope stability. In this study the electrical properties of the ground were measured using electrodes physically inserted into the landslide surface. We ran several thousand simulations of fluid flow to calibrate our modeling parameters against electrical measurements. We found that the moisture content of the slope was sustained at high levels prior to recorded failure events. Hence, we suggest that electrical measurements on landslides could be useful for landslide early warning systems.

1. Introduction

Most landslides are moisture-induced, and represent a significant geohazard resulting in socioeconomic impacts across the globe (Gibson et al., 2013). Increases in pore pressure are known to trigger landslides (Duncan et al., 2014). Furthermore, landslides are likely to become more pervasive due to climate change and the greater prevalence of extreme rainfall events (Fischer & Knutti, 2016). In saturated conditions the resistance to shear is classically considered to be a function of effective stress, rock cohesion and friction angle, where the effective stress is a function of positive pore pressure (Terzaghi, 1936). This concept of pore pressure controlling the stress conditions is also true for unsaturated materials (Bishop, 1959), where pore pressures are negative and linked to the level of moisture in the ground (van Genuchten, 1980). Numerous studies have considered the role of moisture within unstable slopes, citing the importance of estimating the near-surface pore pressures in developing models of unsaturated ground stability (or instability) (Fredlund et al., 1978, 1996; Lu & Godt, 2008; Lu & Likos, 2006).

© 2024. The Author(s). *Water Resources Research* published by Wiley Periodicals LLC on behalf of American Geophysical Union.
This is an open access article under the terms of the Creative Commons Attribution License, which permits use, distribution and reproduction in any medium, provided the original work is properly cited.

19447973, 2024, 10, Downloaded from https://agupubs.onlinelibrary.wiley.com/doi/10.1029/2023WR036319 by British Geological Survey, Wiley Online Library on [04/12/2024]. See the Terms and Conditions (https://onlinelibrary.wiley.com/terms-and-conditions) on Wiley Online Library for rules of use; OA articles are governed by the applicable Creative Commons License

While slope hydrology clearly influences slope stability, the slope geometry and distribution of geological materials in a slope are equally important. In slope stability modeling, knowledge of the subsurface structure is required, which is conventionally derived from boreholes. On the other hand, geophysical techniques offer a non-invasive, spatially sensitive means to rapidly characterize the subsurface and inform ground models (Bichler et al., 2004; Merritt et al., 2013; Moradi et al., 2021). In particular, the sensitivity of geoelectrical properties of the ground to changes in moisture content has made electrical resistivity tomography (ERT) a primary geophysical technique for studying landslides (Pazzi et al., 2019; Perrone et al., 2014; Whiteley et al., 2019). Relationships between the resistivity of rocks and corresponding saturation levels have been understood and explored for decades (Archie, 1942, 1947; Glover et al., 2000; Montaron, 2009; Shah & Singh, 2005; Waxman & Smits, 1968). Consequently, many studies have focused on directly translating electrical images of the ground into hydro-mechanical properties, namely moisture content (Boyd et al., 2024; Holmes et al., 2022; Moradi et al., 2021; Uhlemann et al., 2017). This is done by developing a material-specific petrophysical transfer function, either using field samples that have subsequently been studied under laboratory conditions (Holmes et al., 2020; Merritt et al., 2016), or through infield calibration using point sensors (Crawford & Bryson, 2018). However, translating electrical images into spatial distributions of moisture content does not immediately inform parameters needed for slope stability analysis, such as flow parameters, pore pressures, or shear strengths. Hence there is a growing body of works that has studied translating electrical properties of geological materials into other geotechnical parameters such as negative pore pressure (or matric potential) (Cardoso & Dias, 2017; De Vita et al., 2012; Holmes et al., 2022) and ultimately relating resistivity directly to shear strength (Crawford & Bryson, 2018). An alternative approach is to couple electrical and hydrological flow models to better estimate hydrologic properties of subsurface materials (Binley et al., 2002; Hinnell et al., 2010); in such an approach one does not solve for the electrical properties of the subsurface, but rather the hydrological parameters controlling moisture content in the subsurface.

1.1. Hydrogeophysical Modeling

Given the established links between electrical resistivity and water saturation states in geological materials, electrical geophysics can be used to constrain processes occurring in the unsaturated portion of the near-surface. One of the first such reported studies is that of Binley et al. (2002), where cross borehole ERT and ground penetrating radar are used to constrain hydraulic conductivity in near-surface sandstones by comparing multiple hydrological simulations to geophysical inversions. Subsequently, the term "hydrogeophysical inversion" has been applied to studies where both geophysical and hydrological parameters are solved. There is not a formal workflow coupling the geophysical and hydrological response, but this is typically achieved by widely sampling the parameter space via multiple realizations of hydrological models (Hinnell et al., 2010; Mboh et al., 2012; Pleasants et al., 2022; Tso et al., 2020). Regardless of the coupling mechanism, some statistical values such as root mean square (RMS) error or likelihood value are used to quantify the level of fit between the hydrological and geophysical inputs. The goal of hydrogeophysical inversion is to find a distribution of electrical and hydrological parameters consistent with the observed data. In the context of landslides, it is the hydrological parameters that are most relevant for slope stability modeling.

Hydrogeophysical inversions leverage either uncoupled or coupled mechanisms. In the former case, geophysical measurements are inverted conventionally using a geophysics inverse code (e.g., Binley & Slater, 2020; Johnson et al., 2010; Loke et al., 2013). Geophysical and hydrological models are linked via a petrophysical function to derive fitting statistics (Binley et al., 2002). In contrast, in a coupled approach no conventional inversion of geophysical data takes place, rather the statistical fits of simulated and measured geophysical responses are used to optimize any modeling parameters (e.g., Hinnell et al., 2010; Pleasants et al., 2022; Tso et al., 2020). In the case of Mboh et al. (2012), a global optimizer is used to progressively iterate through different realizations of hydrological modeling parameters until an optimum RMS value is achieved. Whilst both mechanisms (coupled and uncoupled) have merits (Binley et al., 2002; Camporese et al., 2015; Hinnell et al., 2010; Pleasants et al., 2022), the consensus is that coupled modeling approaches are generally superior and therefore solely considered henceforth. Both Hinnell et al. (2010) and Pleasants et al. (2022) report that hydrogeophysical inversions using coupled approaches yielded tighter constraints on resulting hydrological parameters, provided that the hydrological model is appropriate. In this study when testing a synthetic problem to determine saturated hydraulic conductivity, we also found that coupled approaches provided results more consistent with the known

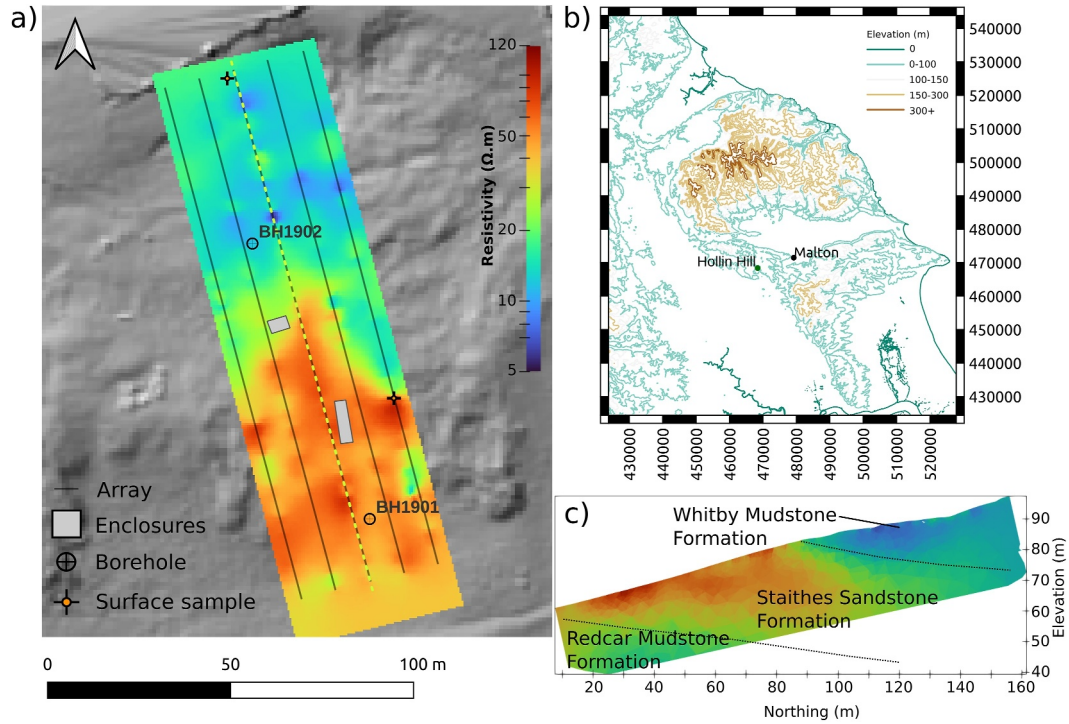

Figure 1. Overview map of field site. (a) Instrument enclosures, sample locations, upper surface of resistivity distribution, as imaged in May of 2016, overlain on a hill shade map of the slope and (b) geographic location (coordinates are given in British National Grid). (c) Shows a 2D resistivity section (also from May 2016) with interpretation for the highlighted electrode array (in yellow). Elements of this Figure have been created using QGIS.

hydrological parameters. It is likely that uncoupled approaches inherently suffer from artifacts in the inversion of geophysical data (due to regularization) (e.g., Carey et al., 2017).

1.2. Motivation and Aims

We study coupled modeling of electrical resistivity and unsaturated flow to determine the posterior distributions of a series of hydraulic parameters, conditioned on time-lapse geophysical data. The motivating factors are twofold: first, the unsaturated soil parameters control the matric potential observed at a given moisture content (Lu & Likos, 2006; van Genuchten, 1980), which in turn controls the shear strength available to the subsurface (Bishop, 1959; Fredlund et al., 1996); second, the selected parameters are necessary for unsaturated flow modeling and determining the pore pressure response of a geological body to rainfall events. Research has shown that deriving unsaturated parameters, via hydrogeophysical coupling, for individual formations is possible (Mboh et al., 2012; Tso et al., 2020). While there has been research into hydrogeophysical modeling of slopes (Pleasants et al., 2022), work has focused on determining singular properties (e.g., density, hydraulic conductivity). Therefore, our research question is whether hydrogeophysical modeling is sensitive to hydrological parameters that could ultimately be used be slope stability modeling. The van Genuchten unsaturated soil parameters, α (alpha) and n, as well as the saturated hydraulic conductivity. We discuss the feasibility of deriving these parameters for synthetic case study where two formations of interest are present and a well-characterized landslide, Hollin Hill (Merritt et al., 2013). Given the importance of these hydrological parameters to slope stability, we further show how these hydrogeophysical outputs may affect models of slope stability, thus demonstrating how geophysical data may have a role in assessing the risk of failure of a slope.

2. Field Site

Hollin Hill (Figure 1) is located approximately 11.5 km west of the town of Malton, in North Yorkshire, UK (latitude/longitude: −0.959586, 54.110784). It has been the subject of long-term geophysical and geotechnical studies (Boyd et al., 2021, 2024; Chambers et al., 2011; Gunn et al., 2013; Merritt et al., 2013, 2016, 2018; Peppa

19447973, 2024, 10, Downloaded from https://agupubs.onlinelibrary.wiley.com/doi/10.1029/2023WR036319 by British Geological Survey, Wiley Online Library on [04/12/2024]. See the Terms and Conditions (https://onlinelibrary.wiley.com/terms-and-conditions) on Wiley Online Library for rules of use; OA articles are governed by the applicable Creative Commons License

19447973, 2024, 10, Downloaded from https://agupubs.onlinelibrary.wiley.com/doi/10.1029/2023WR036319 by British Geological Survey, Wiley Online Library on [04/12/2024]. See the Terms and Conditions (https://onlinelibrary.wiley.com/terms-and-conditions) on Wiley Online Library for rules of use; OA articles are governed by the applicable Creative Commons License

et al., 2019; Uhlemann et al., 2015, 2016, 2017; Whiteley et al., 2020) and is an active slow-moving landslide. The slope is located on the south facing side of a glacial valley of the Howardian Hills and is underlain by Lias Group rocks of the early Jurassic. Toward the top of the slope, which is actively failing, outcrops the Whitby Mudstone Formation (WMF), which is associated with amongst the highest density of landslides of any UK formation (Hobbs et al., 2005). In this case the WMF is actively failing through rotational, translational, and creeping failure. According to the nomenclature of Varnes (1978), the landslide is considered to be complex and slow-moving. Elements of the slope have moved by several meters since 2008 (Boyd et al., 2021; Uhlemann et al., 2017).

2.1. Slope Hydrogeology

As a result of several geophysical and geotechnical studies, Hollin Hill is well-characterized from a geological perspective (Figure 1) to ∼10 m below ground level. The upper part of the slope is composed of WMF, a mudstone unit, which according to particle size analysis is almost entirely composed of clay (63.7%) and silt (36.1%). The lower part of the study area comprises the Staithes Sandstone Formation (SSF), which although named a sandstone is still relatively fine grained, composed of clay (42.0%), silt (41.7%), and finally sand and gravels (16.3%). The SSF is a competent rock and is well-cemented in core samples. The boundary between the WMF and SSF is approximately mid-slope, located below a central plateau. On the other hand, much of the SSF outcrop is concealed by clay-rich earthflow material originating from the WMF further upslope (Figure 1). Above the WMF lies the Dogger Formation, a calcareous sandstone unit that outcrops at the top of the valley and north of the WMF. At the WMF-SSF boundary, a thin layer of ironstone can be observed in borehole records. Below the SSF is the Redcar Mudstone Formation (RMF), which is known to outcrop further south into the valley. The exact depth of the SSF-RMF boundary in the monitoring area is unknown. Geophysical images (Merritt et al., 2013; Uhlemann et al., 2017) a decrease in resistivity at ∼10 m below the SSF (Figure 1). This could be indicative of the underlying RMF, the water table, or both.

The ground model developed for the site, in terms of subsurface structure and lithology, contributes to the current understanding of slope hydrology. Toward the top of the slope, moisture levels remain relatively high in the near-surface, suggesting the presence of a perched water table around the WMF-SSF boundary (Boyd et al., 2021, 2024; Gunn et al., 2013; Uhlemann et al., 2017). The SSF, in contrast, appears to be free draining, and during the winter months a natural spring occurs at the SSF-RMF boundary downslope of the study area, which suggests a significant negative contrast in hydraulic conductivity between the SSF and RMF. An infiltration experiment at Hollin Hill, by van Woerden et al. (2014), reported that the SSF had a hydraulic conductivity an order of magnitude greater than the WMF. In borehole records, ∼1 cm size sand-filled fissures were observed in the SSF unit; hence it is likely that these act as hydrological pathways and allow the SSF to drain freely. Water levels measured in boreholes, close to the central line of the monitoring array (Figure 1), during autumn 2022 show that the water table was maintained at 5–6 m below the ground surface at both the top and bottom of the slope.

2.2. Instrumentation

There are two types of instrumentation at Hollin Hill that are of interest to this study. First, in 2014 a weather station equipped with COsmic-ray Soil Moisture Observing System (COSMOS) instrumentation (Stanley et al., 2019; Zreda et al., 2012) was installed on site. The station records relative humidity, wind speed, and local volumetric moisture content (VWC). This allows the computation of potential evapotranspiration via the Penman-Monteith method (Allen et al., 2006). As such, consistent rainfall records for the site exist from April 2014 onwards. Potential evapotranspiration estimations are available for the slope at daily intervals (Stanley et al., 2019).

Second, in 2008 a geoelectrical monitoring system was installed on the slope (Figure 1a), an automated time-lapse electrical resistivity tomography (ALERT) instrument (Kuras et al., 2009; Ogilvy et al., 2009), monitoring over a 5 by 32 grid array of electrodes. The longest axis of the array is parallel to the slope (Figure 1). Dipole-dipole (DD) measurement configurations (Binley & Slater, 2020) are used to record transfer resistance (TR) and take place every 2 or 3 days during normal operation of the instrument. TR measurements are made remotely on an automated schedule and uploaded to a long-term data storage solution via telemetry. The full specification and justification of the DD arrays are documented in Merritt et al. (2018) and Uhlemann et al. (2017). The ALERT

19447973, 2024, 10, Downloaded from https://agupubs.onlinelibrary.wiley.com/doi/10.1029/2023WR036319 by British Geological Survey, Wiley Online Library on [04/12/2024]. See the Terms and Conditions (https://onlinelibrary.wiley.com/terms-and-conditions) on Wiley Online Library for rules of use; OA articles are governed by the applicable Creative Commons License

system ran until 2018, albeit with significantly reduced data quality toward the end of its operational lifetime (Boyd et al., 2021), and was replaced by a successor system in 2020.

3. Modeling and Calibration

To perform a coupled hydrogeophysical inversion a mechanism to model both the hydrological and geoelectrical responses of the ground is required. Because unsaturated conditions are present in the near-surface of the field site, the variably saturated flow simulator SUTRA (Provost & Voss, 2019) has been employed. Additionally, SUTRA is open source and a self-contained program with a proven history for use within research, which is beneficial to manipulating the program for coupled modeling. Likewise, for the resistivity modeling component of this paper the R2 code (Binley & Slater, 2020) is used. It is closed source, but the program is freely available, self-contained, and a well-established code for modeling ERT data.

For the purposes of this study the investigation is 2D (two-dimensional), however the hydrological and geophysical modeling computations have a pseudo 3D component to them. While a full 3D study is theoretically viable, the computation time and complexity required in the conceptual hydrological model are far greater than in 2D, which was deemed not to be practical. The 2D section of interest is the center line of the monitoring array (highlighted in Figure 1), as this does not intersect parts of the slope moving regularly.

3.1. Physical Property Calibrations

To couple the hydrological and geophysical response of the ground with respect to rainfall, we employ petrophysical relationships between electrical resistivity and saturation, a hydrological state which is computed by SUTRA. Additionally, as the resistivity of geological materials is sensitive to temperature, we apply a seasonal temperature correction to the modeled resistivities.

3.1.1. Petrophysical Relationships

Petrophysical relationships for the rocks of Hollin Hill are complex. Clay minerals introduce an electrically conductive "double layer" to the rock matrix, which conduct electricity in addition to any pore fluid (Waxman & Smits, 1968). Moreover, the shrink-swell properties of the mudstones means that porosity is variable, increasing with higher moisture content. We collected borehole samples from the WMF and SFF (Figure 1) and measured a range of gravimetric moisture contents and resistivity directly. An additional complexity is the anisotropy of the resistivity response of samples in relation to sedimentary structures (Boyd et al., 2024; Merritt et al., 2016). Porosity changes with moisture content were measured with a SHRINKiT system (Hobbs et al., 2010), which allowed us to convert measurements made in gravimetric moisture content (GMC) to saturation (see Supporting Information S1, Section A). We found that a power law adequately described the relationship between resistivity, ρ, and saturation, S, for the purposes of this study, where

$$\rho = \frac{1}{(a[S^b])} + c. \tag{1}$$

Here a, b, and c are fitting parameters found through a least squares approach (Virtanen et al., 2020). Given the high clay content of the material, the equations put forward by Waxman and Smits (1968) and those by Montaron (2009) were explored, but ultimately a generic power-law fit best described the measured data. It could be that physical processes are occurring in the material that are not captured by published petrophysical relationships, hence a variable porosity was accommodated in our Waxman Smits formulation, although the result was unsatisfactory for the SSF. The fitting parameters used for the petrophysical relationships are shown in Table 1 and Figure 2. Testing was completed in a temperature-controlled laboratory at 20°C, and the water used to wet samples was de-aired and de-ionized to best simulate rainwater infiltration (given the allowed equilibration within the sample).

We retrieved samples from ∼1.5 m depth in the SSF (borehole 1901 in Figure 1a) and made resistivity measurements both parallel and perpendicular to the bedding. Our objective was to find a petrophysical relationship that could be used in coupled modeling and represented field conditions as best as possible. Fitting petrophysical relationships individually to the parallel and horizontally aligned measurements yielded better fitting statistics than a combined fit, but we found the magnitude of apparent resistivities in the field closely matched that of a

Table 1
Fitting Parameters Used in Equation 1 for the Relationship Between Saturation and Resistivity (Ωm) for Hollin Hill Samples

Formation	*a*	*b*	*c*	χ^2	*r*	*n*	Samples
SSF	0.10	3.58	29.34	187.05	0.50	55	2
WMF	0.42	2.14	4.11	4.35	0.95	66	2
WMF (shallow)	1.53	17.51	14.61	4.91	0.95	66	2

Note. Parameters *a*, *b*, and *c* are unitless. The number of measurements, *N*, for each formation type is shown, Chi-squared and Pearson's correlation coefficient *r* are also shown.

combined fit. This suggests that infield resistance measurements are sensitive to a mix of electrical currents flowing in both the vertical and horizontal orientation. Given this hypothesis, we used a combined fit as the petrophysical relationship to describe SSF's response to various moisture levels (Figure 2).

Regarding the WMF, we retrieved samples from borehole cores at 1, 4, and 6 m depths (denoted 1902 in Figure 1a). We found that the samples retrieved from 4 to 6 m depth exhibited anisotropy and are generally more resistive when current is passed vertically across bedding planes. However, the sample retrieved from 1 m depth was more resistive still, even at higher moisture contents, and isotropic regarding measured resistivities and orientation of current flow. Chemical weathering and shallow movements have likely removed any sedimentary structures from the shallow WMF resulting in isotropic electrical properties. Hence, a different petrophysical relationship was applied to the WMF in the upper 1 m of the modeling domain in the field case study. For the "deep" WMF (>1 m depth) we chose to use electrical resistivity measurements made when current flows horizontally to bedding planes to form our petrophysical relationship, as we found these best match in-field measurements of apparent resistivity made over the WMF.

A critical petrophysical parameter is the formation porosity, which (as previously mentioned) is challenging to quantify in materials from Hollin Hill. A prior hydrological study (van Woerden et al., 2014) found the porosity of the WMF to be 48% and residual VWC of 10%; equivalent values for the SSF were 38% and 6%, which are adopted for hydrological simulation. However, the porosity measurement in shrink swell-prone clays merits further discussion.

3.1.2. Unsaturated Moisture Retention Curve

In SUTRA we used a van Genuchten (1980) curve to describe the relationship of effective saturation to matric potential (negative pore pressure),

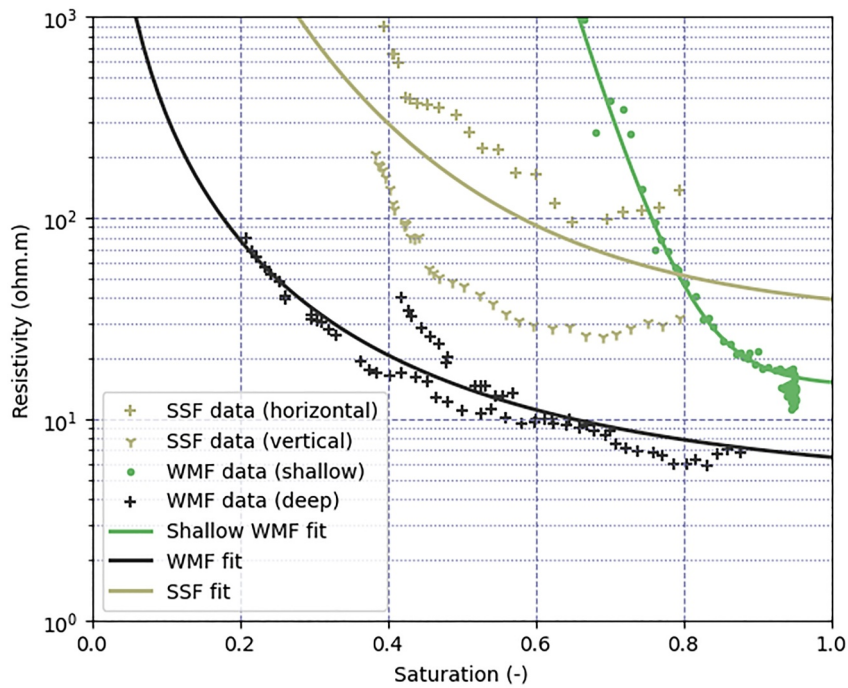

Figure 2. Petrophysical calibration of saturation and resistivity, showing fitted curves for Whitby Mudstone Formation (WMF) and Staithes Sandstone Formation (SSF) as well as measured data points for the 6 samples documented in Table 1.

19447973, 2024, 10, Downloaded from https://agupubs.onlinelibrary.wiley.com/doi/10.1029/2023WR036319 by British Geological Survey, Wiley Online Library on [04/12/2024]. See the Terms and Conditions (https://onlinelibrary.wiley.com/terms-and-conditions) on Wiley Online Library for rules of use; OA articles are governed by the applicable Creative Commons License

Table 2
Parameters Used for Correcting Forward Modeled Resistivities From a Reference Temperature

Parameter	T_{mean} (°C)	ΔT (°C)	d (M)	φ	T_{ref} (°C)
Value	10.03	15.54	2.26	−1.91	20

Note. Adapted from Uhlemann et al. (2017).

$$S_e = \frac{S - S_r}{S_s - S_r} = (1 + [\alpha h]^n)^{-m}, \quad (2)$$

where: h is matric potential in m; S_e is effective saturation; α and n are fitting parameters and we set $m = 1 - 1/n$ (van Genuchten, 1980); S_s is the maximum saturation value (1); S_r is the residual saturation. S_r can be approximated by dividing the residual VWC value by the formation porosity (which is assumed constant in SUTRA). We compute relative hydraulic conductivity (or permeability), k_r, as function as of S_e (van Genuchten, 1980),

$$k_r(S_e) = \sqrt{S_e} \cdot \left(1 - \left[1 - S_e^{\frac{1}{m}}\right]^m\right)^2. \quad (3)$$

3.1.3. Temperature Correction

Electrical conductivity (the inverse of resistivity) is affected by temperature, and increases by approximately 2% per one degree increase in temperature when above 0°C (Hayley et al., 2007). Previous geophysical investigations of Hollin Hill (e.g., Boyd et al., 2021) used a seasonal temperature-depth model documented by Uhlemann et al. (2017) whereby the temperature at a given depth and day during the year is based on the diffusive heat equation (Brunet et al., 2010),

$$T_{model}(z,t) = T_{mean} + \frac{\Delta T}{2} \exp\left(-\frac{z}{d}\right) \sin\left(\frac{2t\pi}{365} + \varphi - \frac{z}{d}\right). \quad (4)$$

Here T_{mean} is the average annual air temperature, ΔT is the difference between the largest and smallest annual temperatures, φ is a phase offset to bring surface and air temperature into phase, d is characteristic depth and defined as the depth where ΔT has decreased by $1/e$ (Brunet et al., 2010), t is the day during the year and z is depth of the barycenter of each cell in the modeling mesh. Uhlemann et al. (2017) found the relevant parameters for Hollin Hill to compute Equation 5 and we list them in Table 2. Normally resistivity is corrected according to a ratio model (Ma et al., 2011). In the above studies, inverted resistivities were corrected to a reference value (usually 20 or 25°C); by contrast in our case resistivities need to be corrected from a reference value of 20°C to a modeled temperature. We "corrected" our resistivity according to the following relation,

$$\rho_0 = \frac{\rho_{ref}}{\left[1 + \frac{c_t}{100}(T_{ref} - T_{model})\right]}, \quad (5)$$

where ρ_{ref} is the resistivity (in Ωm) at reference temperature T_{ref} in °C; c_t is the percentage change in resistivity per degree, set at −2%/°C; ρ_0 is the corrected resistivity.

3.2. Forcing Data

Our hydrological forcing (or driving) data is recorded by the weather station on the slope, which is publicly available (Stanley et al., 2019). The infiltration rate is effective rainfall, that is, measured rainfall minus the effects of evapotranspiration. We followed the suggestions of Allen et al. (1998) for computing our effective rainfall estimations (See Section B of Supporting Information S1). We used a 2.5-year-long rainfall data series, spanning June 2014 to December 2016 (Figure 3). We also extracted time-lapse DD measurements from January 2015 to December 2016 from the central, downslope, array of the geoelectrical monitoring (ALERT) system (highlighted in Figure 1a). This monitoring period includes good quality ERT data that overlaps with COSMOS data availability; additionally significant movements were observed on the slope in April 2016 (Boyd et al., 2021), and hence this period is interesting for investigating slope dynamics. We ran our SUTRA models at a 1 day temporal resolution for 3 years and started modeling respective geophysical responses after 1 year. For the first 6 months of modeling the infiltration rate was set at the average effective rainfall, 0.4 mm/day. The following 6 months are real hydrological data, thus allowing the hydrological model time to "warmup" prior to hydrogeophysical coupling.

19447973, 2024, 10, Downloaded from https://agupubs.onlinelibrary.wiley.com/doi/10.1029/2023WR036319 by British Geological Survey, Wiley Online Library on [04/12/2024]. See the Terms and Conditions (https://onlinelibrary.wiley.com/terms-and-conditions) on Wiley Online Library for rules of use; OA articles are governed by the applicable Creative Commons License

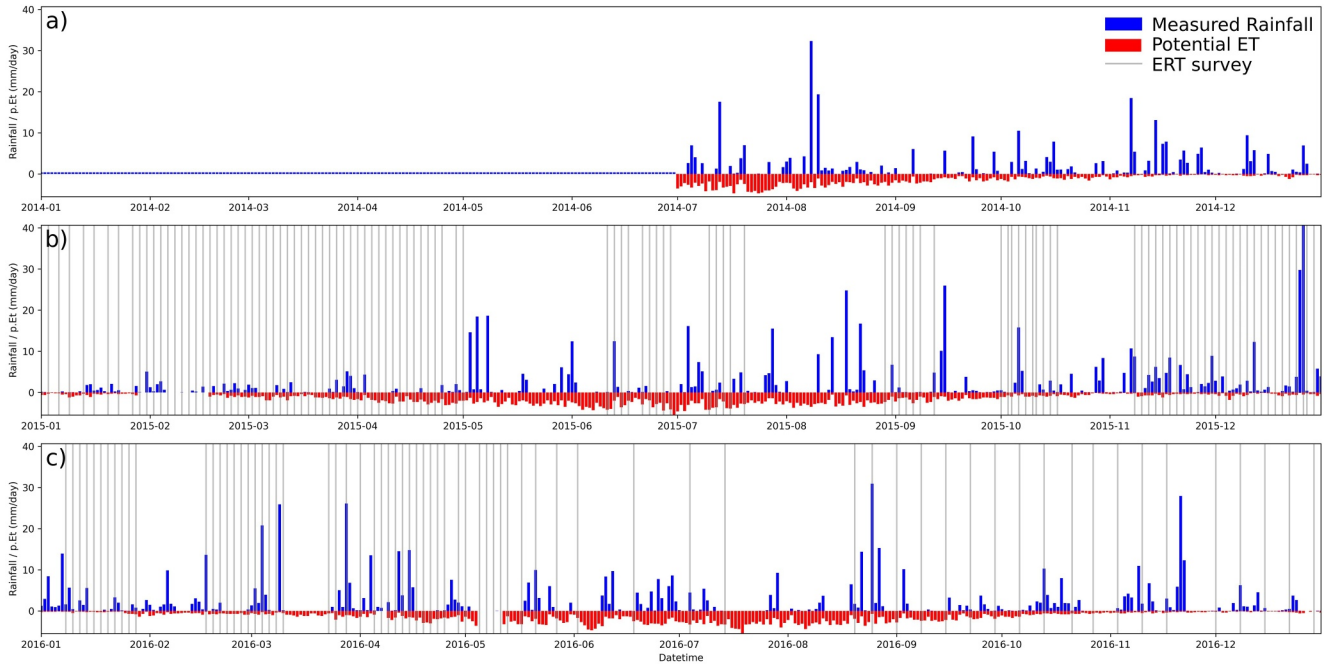

Figure 3. Measured rainfall and estimated evapotranspiration for the period of interest in this study as measured by the weather station located on Hollin Hill (Stanley et al., 2019). Gray lines show the temporal position of electrical resistivity tomography (ERT) surveys.

We rejected TR measurements with a contact resistance over 5 kΩ or reciprocal error greater than 5%. Measurement error estimations are made by fitting a reciprocal error model (Blanchy et al., 2019) to each TR set. Geophysical responses were modeled only when a measurement set was available for a given day in the modeling period, a total of 184 time-lapse DD surveys (Figure 3).

3.3. Hydrogeophysical Coupling

To perform the hydrogeophysical inversion one must generate numerous realizations of hydrological models. This can be done via global optimization (Mboh et al., 2012), a grid search (Pleasants et al., 2022) or Monte Carlo approaches (Hinnell et al., 2010; Tso et al., 2020). However, some of these approaches do not scale well with additional model parameters, as these increase the number of realizations required exponentially. In this case, we are attempting to constrain the van Genuchten (1980) α and n parameters and hydraulic conductivity for the WMF and SSF. We therefore used an adaptive Markov chain Monte-Carlo (McMC) approach (Hastings, 1970) to search the parameter space in six dimensions. Briefly, Markov chains explore the parameter space by proposing new parameters which are drawn (at random) from a prior probably density function (PDF). Each proposed model is compared against the measured data to compute a likelihood value; at each step, if the likelihood is greater than that of the current model parameters, the new parameters are accepted with a probability of 100%, otherwise, the model is accepted with a probability which is the ratio of the proposed and current likelihood (see Section C of Supporting Information S1 for further details). Often many iterations are required to get to part of the parameter space with the desired likelihood value; these iterations are usually referred to as "burn in." In this case, the model output and data are a time series of TR data. To initiate our McMC chains we randomly sampled the entire parameter space for the first proposed model. If the proposed model was unstable (i.e., did not converge), then another model was proposed until a stable set of parameters was found.

To propose a model, parameters were drawn (randomly) from a normal distribution about the currently accepted model parameters, whereby the step size describes the standard deviation associated with the distribution. Ideally, the step size used in the model proposals is calibrated via multiple and completed McMC runs to get the desired acceptance rate. However, as individual simulations can take several minutes finding an appropriate step size through trial and error would be prohibitive. Hence the Metropolis-Hastings algorithm (Hastings, 1970) was adapted to target an acceptance rate of 23.4%, as this is generally considered to be optimal (Gelman et al., 1997; Roberts & Rosenthal, 2001); see Equations S9 and S10 in Supporting Information S1 (Supporting Information S1,

19447973, 2024, 10, Downloaded from https://agupubs.onlinelibrary.wiley.com/doi/10.1029/2023WR036319 by British Geological Survey, Wiley Online Library on [04/12/2024]. See the Terms and Conditions (https://onlinelibrary.wiley.com/terms-and-conditions) on Wiley Online Library for rules of use; OA articles are governed by the applicable Creative Commons License

19447973, 2024, 10, Downloaded from https://agupubs.onlinelibrary.wiley.com/doi/10.1029/2023WR036319 by British Geological Survey, Wiley Online Library on [04/12/2024]. See the Terms and Conditions (https://onlinelibrary.wiley.com/terms-and-conditions) on Wiley Online Library for rules of use; OA articles are governed by the applicable Creative Commons License

Section C). Each Markov chain was allowed to run for 1,000 iterations; we ran 12 chains in parallel on a multicore processor for a total of 12,000 model proposals. Note that the results of McMC approaches do not yield model parameters specifically, but rather a posterior PDF of parameter proposals that maximize the likelihood. To test the normality of our McMC results we employ the Shapiro-Wilk test statistic (Shapiro & Wilk, 1965); which scales between zero and one, the former rejects any normality whilst the latter indicates normality. Studies indicate that the Shapiro Wilk test is a reliable test of normality (Razali & Wah, 2011) and coded implementations are readily available (Virtanen et al., 2020).

3.3.1. Computation Specifics

The base version of SUTRA 3.0 requires the software to be recompiled by the user for different unsaturated soil parameters. This enables users to define their own relationships between saturation, matric potential, and relative hydraulic conductivity, although in this case compiling SUTRA for each hydrological model realization would create significant computational overhead. Hence, we modified the SUTRA source code to accept unsaturated soil parameters as a dynamic input. The geoelectrical modeling code, R2, was unmodified. To couple R2 and SUTRA, we created a custom object-orientated approach in Python (Van Rossum et al., 2009). We ran our problem on a Windows 11 Pro operating system, which spawned Markov chains in parallel. Each parallel McMC run would take several days to run on an AMD 5900x processor.

3.3.2. Boundary Conditions and Meshing

In R2 all external boundaries of the mesh are treated as Neumann boundaries, that is, electrical current may not flow in or out of the model at the boundaries of the mesh (Binley & Slater, 2020). To characterize electrical current flow accurately in an unconstrained half-space, the mesh boundaries are treated as pseudo-infinite. We used a triangular mesh for geoelectrical modeling as it allows for efficient discretization of the mesh near electrodes and at external mesh boundaries, reducing computational overhead. For SUTRA we used a quadrilateral mesh (Figure 4a), both the synthetic and field case study had the same boundary conditions. The base of the mesh was held at a minimum pore pressure to set the water table at ∼5 m below the ground surface (as shown by borehole investigations) and prevent the pooling of fluid in the domain. The vertical downslope edge was set as a seepage boundary, allowing for fluid to leave the model. Furthermore, the top surface of the mesh was set as a source/sink boundary from which fluid enters the mesh, in this case, the fluid input (infiltration) was effective rainfall. We also found that allowing seepage (fluid to exit at atmospheric pressure) at the top of the modeling domain improved model stability. By using different modeling domains for the geoelectrical and hydrological modeling, we were able to minimize the overhead associated with solving the forward problem for both scenarios respectively and ensure the boundary conditions are sufficient for both modeling approaches. A linear interpolator (Virtanen et al., 2020) maps geoelectrical properties in the hydrological modeling domain. We set up SUTRA to output per-element saturation calculations at each time step in the hydrological model, which can be directly converted into resistivity via Equation 1.

3.4. Other Field Data

Boreholes at Hollin Hill facilitate water level logging and slug tests. In borehole 1901 (Figure 1), which intersects the SSF, the water table is logged at 5.7 m below ground level (bgl) and the measured hydraulic conductivity is 0.64 m/day. At borehole 1902 (Figure 1) the water table is logged at 5 m bgl, unfortunately the borehole casing has been warped by slope movements and is not suitable for slug tests. However, surface infiltration experiments at Hollin Hill show that the near-surface WMF has a hydraulic conductivity of 0.013 m/day (van Woerden et al., 2014). Some limited testing of WMF core samples in a HYPROP 2 device (METER Group Inc.) is also available, which provides laboratory-derived values of the unsaturated soil parameters. Five samples are taken from the flow lobes and exposed backscarp for this investigation. Through curve fitting (Equation 2) of matric potential and GMC measurements (2,218 useable for analysis), using an McMC approach, we found the estimated n and α values are 1.61 ± 0.11 (–) and 0.040 ± 0.029 m^{-1} respectively for the WMF (See Figure S1 in Supporting Information S1). The SSF is not exposed at the surface, making retrieving physical specimens for that formation more difficult. A borehole sample was run through the HYPROP but cavitated early in the experiment, hence the results were unreliable for curve fitting.

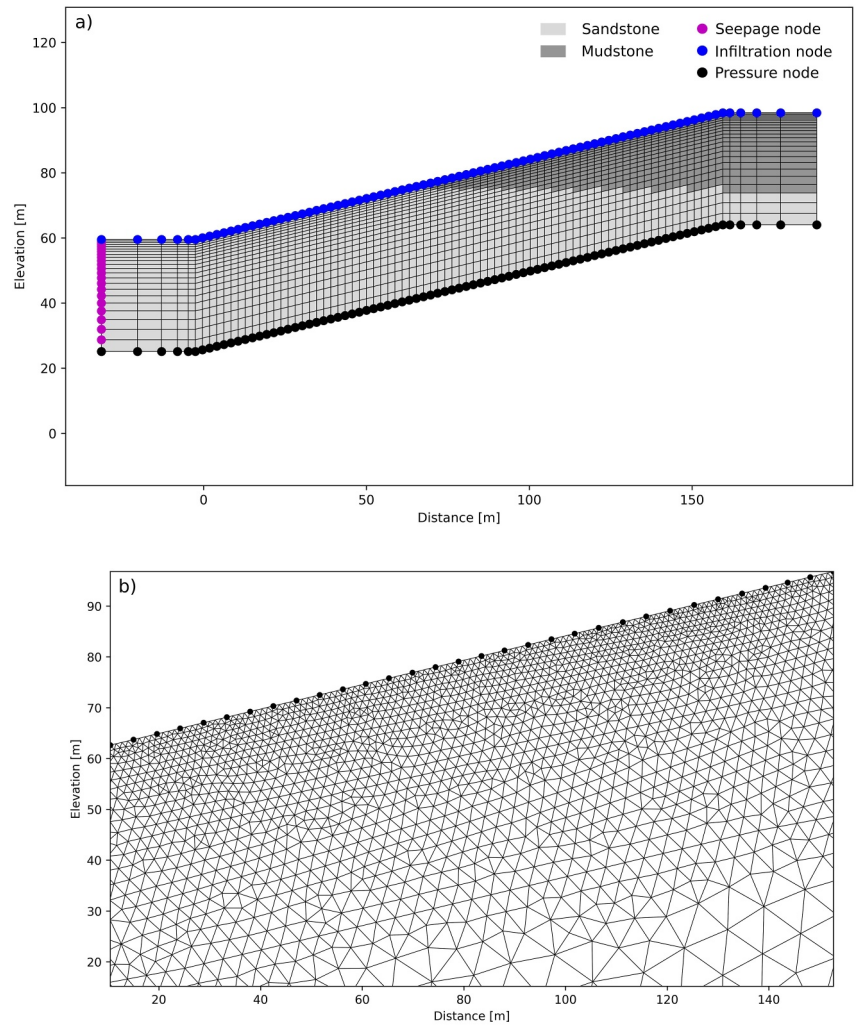

Figure 4. Modeling domain for SUTRA (a) and R2 (b) in the case of modeling a synthetic scenario. Note that for (b) the modeling domain extends beyond the edges of the image.

4. Analysis

4.1. Synthetic Case

A synthetic case was designed to confirm that the hydrogeophysical modeling is sensitive to the van Genuchten (1980) α and n parameters as well as hydraulic conductivity, K. We used the same hydrological forcing and measurement schemes as those at Hollin Hill but using a simplified hill slope geometry. In this model there is an upper layer with a hydraulic conductivity of 0.013 m/day and a lower layer with 0.64 m/day analogous to the sandstone present at Hollin Hill. We converted hydraulic conductivity to permeability for simulation inside of SUTRA (Section B of Supporting Information S1). Figure 4 shows the setup of the hydrological modeling domain and boundary conditions. In SUTRA, fluid input is defined at source nodes in terms of kg/s (Equation S5 in Supporting Information S1); we used generalized flow nodes (Provost & Voss, 2019) to allow seepage on the left-hand side, and at the source/sink nodes at the top, of the modeling domain (Figure 4a). A minimum pore water pressure is forced along the bottom of the domain to prevent pooling. Note that the right-hand side of the slope is an inactive (or no flow) boundary.

We ran a warmup period for the model over 6 months to get a starting distribution of stable pore pressures and then ran hydrological forcing for 2.5 years using the effective rainfall as input. Finally, we simulated the resistivity response for 2 years as in the real scenario and used the same petrophysical transfer functions between saturation and resistivity. For the DD schedule, we use the same measurement sets as the filtered data and simulate the data for

19447973, 2024, 10, Downloaded from https://agupubs.onlinelibrary.wiley.com/doi/10.1029/2023WR036319 by British Geological Survey, Wiley Online Library on [04/12/2024]. See the Terms and Conditions (https://onlinelibrary.wiley.com/terms-and-conditions) on Wiley Online Library for rules of use; OA articles are governed by the applicable Creative Commons License

19447973, 2024, 10, Downloaded from https://agupubs.onlinelibrary.wiley.com/doi/10.1029/2023WR036319 by British Geological Survey, Wiley Online Library on [04/12/2024]. See the Terms and Conditions (https://onlinelibrary.wiley.com/terms-and-conditions) on Wiley Online Library for rules of use; OA articles are governed by the applicable Creative Commons License

Table 3
Hydrological Modeling Parameters Used in SUTRA; Hydraulic Conductivity (K), Residual and Saturated Moisture Content Values (θ_r and θ_s Respectively), Alpha (α), and n

Unit	K (m. day^{-1})	θ_r (–)	θ_s (–)	α (m^{-1})	n (–)
Sandstone	0.640 (0.0064–6.4)	0.06	0.38	0.2 (0.002–2.0)	1.9 (1.1–2.5)
Mudstone	0.013 (0.0013–0.13)	0.10	0.48	0.1 (0.002–2.0)	1.5 (1.1–2.5)

Note. The bracketed values indicate the parameter space range Markov chain Monte-Carlo chains were able to draw model parameter proposals from.

same time increments (Figure 3). The parameters for the sandstone and mudstone analogues are shown in Table 3. For computing our likelihood values at each McMC iteration we assume 2% data error in synthetic TR values, which is comparable to the level of error we observed for transfer resistances measured by ALERT.

The van Genuchten water retention parameters, α and n values, can vary significantly between similar small-grained soil and rock types (Thakur et al., 2005; van Genuchten, 1980). Hence, we selected parameters in a way that would encourage the SSF analog to remain at a low water content, as implied by ERT processing (Boyd et al., 2021; Uhlemann et al., 2017), while the WMF analog remains at relatively high water content during SUTRA simulations. It is important to note that for the synthetic model setup we did not need to apply any temperature corrections and can assume that all resistivities are taken at their reference value (20°C) Furthermore, values of α and K can vary by orders of magnitude, hence they are sampled in $\log_{10}$ space. K is allowed to vary by an order of magnitude smaller and larger about the known values.

4.1.1. Results

The results of the McMC runs are 6-dimensional (3 parameters × 2 formations), hence we visualize the results in three different panels for the two zones in the modeling domain (Figure 5). Means and standard deviations are calculated for resulting McMC samples (Table 4), however we observed a mix of bimodal and normally distributed posterior PDFs that must be considered additionally and merits further discussion. Indeed allowing for bimodal distribution was required for obtaining a stable curve fit in some cases (Figure 5). The results show that the part of the parameter space that maximizes the likelihood corresponds to the actual known values (Table 4). We filter "burn in" on successful chains such that only the last 750 iterations of each chain can be considered for PDF analysis, furthermore curve fitting, and statistics, are calculated in the log domain in the case of α and K. McMC chains appear to converge reasonably well for the van Genuchten parameters, but not in the case of hydraulic conductivity.

4.2. Field Case

The general setup of the model is the same as the synthetic case but with different geometry (Figure 6) and an additional layer to represent the RMF. We extracted surface topography from an appropriate digital elevation model of Hollin Hill (Boyd et al., 2021). The subsurface geometry is derived from 2D geophysical sections of the slope (Figure 1c).

The hydraulic parameters for the WMF and SSF used in the hydrological modeling are presented in Table 5. Little is known about the hydraulic properties of the RMF, however the resistivities resemble those of the WMF in geoelectrical images, therefore we assume that the unsaturated soil properties, and petrophysical relationships, are the same for the RMF as the WMF. The exception is the hydraulic conductivity of the RMF, which is set to the same value as that of the SSF (0.64 m/day); we found this necessary for numerical stability in SUTRA and to drive realistic changes in near-surface saturations in the upper part of the modeling domain. Likewise, HYPROP experiments on WMF samples (recovered from the backscarp area) were used to populate the unsaturated soil retention parameters for the RMF (Table 5) as these are necessary for hydrological modeling, although practically the formation is mostly below the water table so retention parameters will have little impact on the results. Once more, sampling of α and K are performed in the log domain (to the base of 10).

We assume that the values of α and n have a uniform prior PDF, values shown in Table 5. Model proposals are drawn from a Gaussian distribution with a step length set at 0.1 for all parameters (the same step length is used in the log domain).

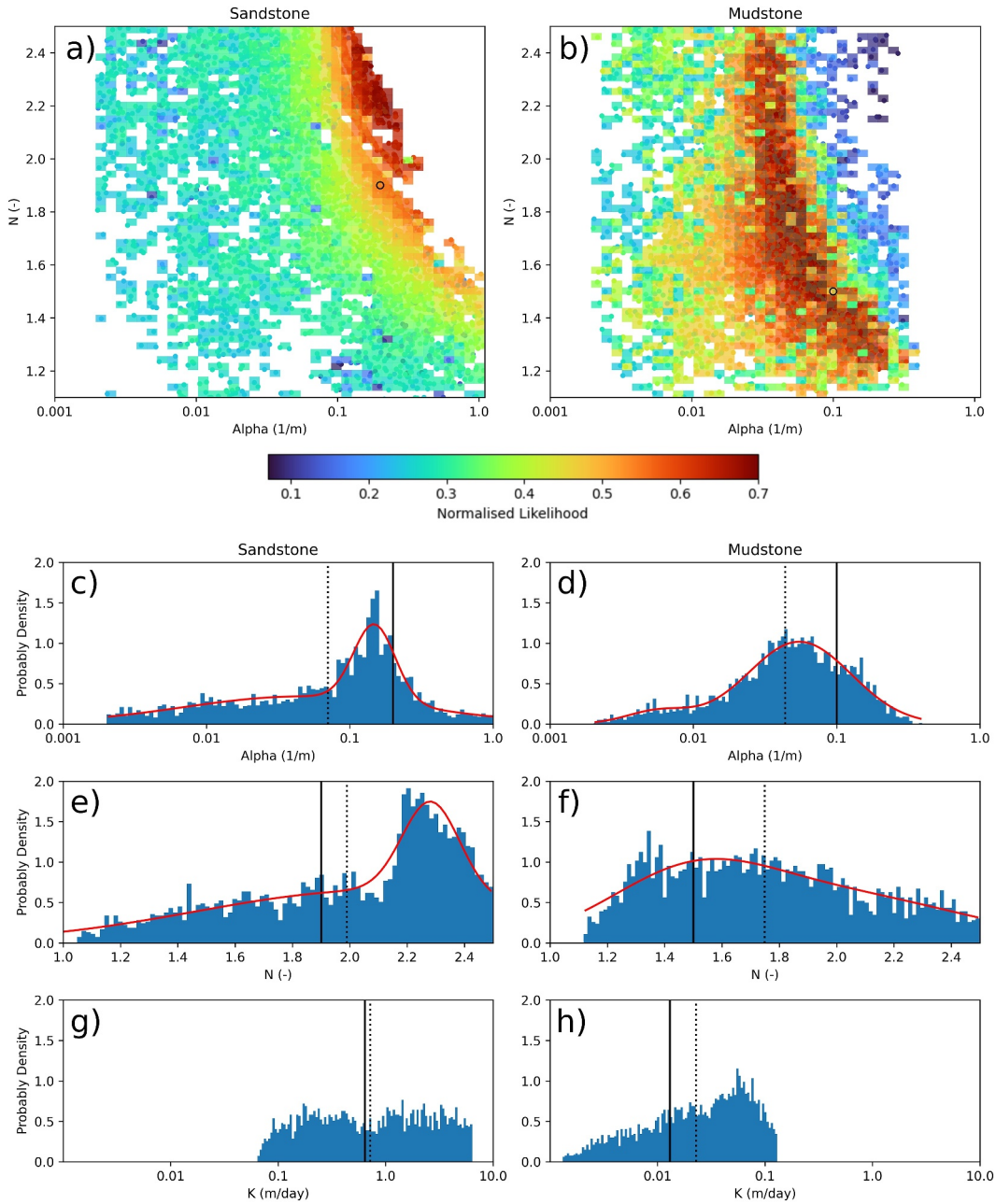

Figure 5. Results of Markov chain Monte Carlo (McMC) chains for a synthetic case study showing the intensity and likelihood values for (a) a sandstone analog and (b) a mudstone analog. Black circles indicate the position of known parameter values. Plots (c)–(h) shows the probability density histograms of the 6 fitted parameters. Red lines show the probably density functions which are a mix of Gaussian and bimodal curves. Black lines indicate the position of known values and dashed lines indicate the means of the McMC parameter samples.

4.2.1. Results

Multiple McMC chains converged on discrete parts of the parameter space, showing the coupled approach is sensitive to the α and n parameters (Figure 7), but less so to K. We observe a mix of normal and bimodal PDFs in the results however, which merit further discussion. Mean and standard deviation statistics are presented in Table 6 (where parameters were sampled in the log domain then the statistics are computed likewise). As with the synthetic case, "burn in" is filtered for the purposes of fitting a PDF.

19447973, 2024, 10, Downloaded from https://agupubs.onlinelibrary.wiley.com/doi/10.1029/2023WR036319 by British Geological Survey, Wiley Online Library on [04/12/2024]. See the Terms and Conditions (https://onlinelibrary.wiley.com/terms-and-conditions) on Wiley Online Library for rules of use; OA articles are governed by the applicable Creative Commons License

Table 4
Means and Standard Deviations for the Sampled Parameters Shown in Figure 5

Unit	$\log_{10}$ (K (m. day^{-1}))	W (K)	$\log_{10}$ (α (m^{-1}))	W (α)	n (–)	W (n)
Sandstone	−0.15 ± 0.55	0.95	−1.15 ± 0.60	0.95	1.98 ± 0.38	0.94
Mustone	−1.64 ± 0.48	0.96	−1.36 ± 0.43	0.98	1.74 ± 0.34	0.97

Note. W refers to the normality statistic according to Shapiro and Wilk (1965) for K, α, and n respectively. The sample size is 3,342.

4.3. Further Analysis

4.3.1. Hydro-Mechanical Modeling

To interrogate how the hydrogeophysical modeling outputs relate to reality we ran 1,000 further realizations of the hydrological model of Hollin Hill presented in Section 4.2. Given that the McMC sampling is apparently insensitive to hydraulic conductivity, the posterior PDF curves shown in Figure 7 were used to randomly sample α and n parameters, while the values of 0.64 and 0.013 m/day are used for K in the SSF and WMF respectively. Of 1,000 simulations, 791 yielded stable results.

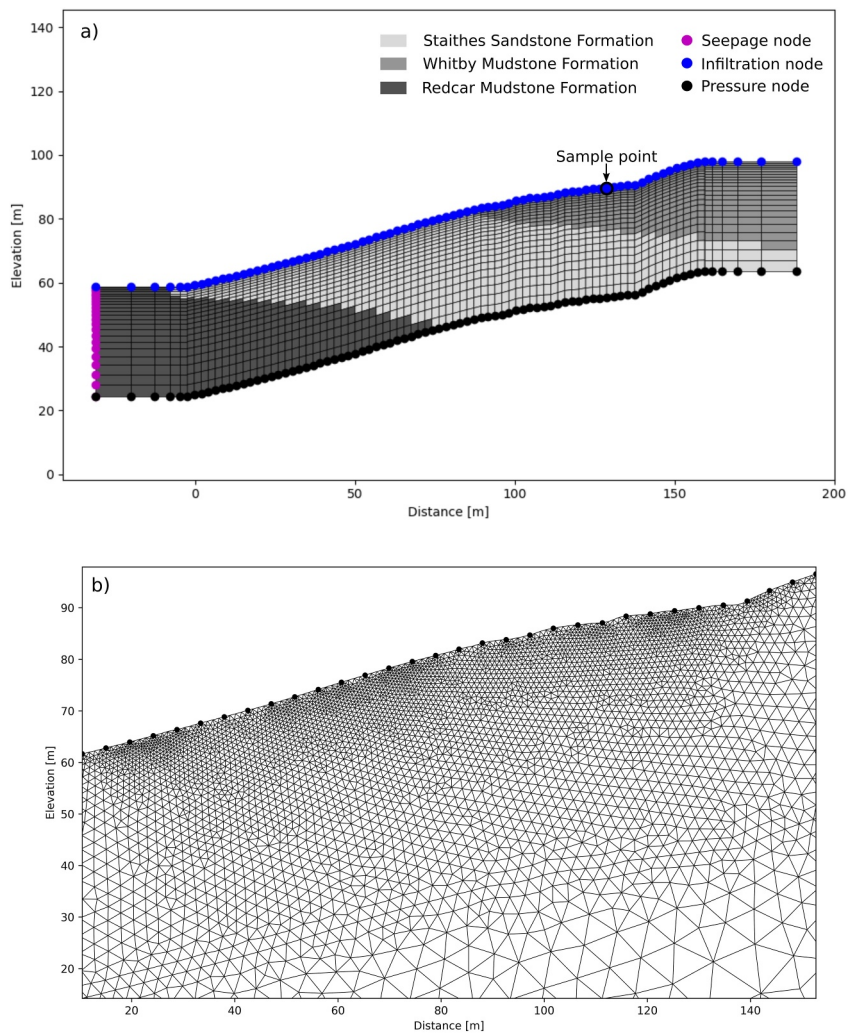

Figure 6. Modeling domains for (a) SUTRA and (b) R2 for purposes of developing a coupled hydrogeophysical model of Hollin Hill. Note that for (b) the modeling domain extends beyond the edges of the image. Also, a sampling point is indicated in the mudstone formation, which is cited later in this manuscript.

19447973, 2024, 10, Downloaded from https://agupubs.onlinelibrary.wiley.com/doi/10.1029/2023WR036319 by British Geological Survey, Wiley Online Library on [04/12/2024]. See the Terms and Conditions (https://onlinelibrary.wiley.com/terms-and-conditions) on Wiley Online Library for rules of use; OA articles are governed by the applicable Creative Commons License

Table 5
Hydrological Modeling Parameters Used in SUTRA and Parameter Ranges of Markov Chain Monte Carlo Parameters

Unit	K (m. day^{-1})	θ_r (–)	θ_s (–)	α (m^{-1})	n (–)
SSF	(0.064–6.4)	0.06	0.38	(0.002–2.0)	(1.1–2.5)
WMF	(0.0013–0.13)	0.10	0.48	(0.002–2.0)	(1.1–2.5)
RMF	0.64	0.10	0.48	0.012	1.44

Note. Values in brackets show the parameter space limits.

Due to the critical links between rainfall infiltration, slope hydrology and shear strength, studies exploring coupled geomechanical and hydrological modeling have become increasingly widespread in recent years (e.g., François et al., 2007; Tacher et al., 2005; Yang et al., 2017), to the point that such approaches are available in commercial software (Galavi, 2010). The aim of such modeling is to solve for geotechnical states, such as shear strength, and hydrological parameters simultaneously. In this case, we briefly discuss hydrological modeling properties in terms of their Atterberg limits. The plastic limit of a clay-rich material is the moisture content at which it undergoes permanent deformation if put under external stresses; additionally, the limit is associated with the point at which a clay material exhibits residual shear strength (rather than peak strength). We estimated the GMC of the WMF from the saturation values shown in assuming a dry density of 1.3 g/cm^3, which we derived from borehole core in the WMF taken at 1.65 m below ground surface. We also found that the plastic limit of WMF material from borehole samples has a value of 34% with laboratory testing. Moreover Merritt et al. (2013) found that the plastic limit of clay-rich Hollin Hill material ranges from ∼33% to 42%.

Figure 8a shows a comparison of estimates of GMC and plastic limits to slope movements; these were measured on a grid of marker pegs installed on the slope for the purposes of tracking movement (Boyd et al., 2021; Uhlemann et al., 2015), via periodic real-time kinematic global positioning surveys. Isolating the peg movements to those in the vicinity of a rotational backscarp that developed during late spring of 2016 (Figure 8a), we observe that meter-scale movements were measured after the WMF apparently reached its plastic limit (of 34%) for 100% of simulations in the winter period between 2015 and 2016 (Figure 8b). High moisture contents are sustained into spring, spiking prior to the date of recorded movement and development of the rotational backscarp feature (Figure 8c).

4.3.2. Resistivity Modeling

As a point of comparison between the hydrogeophysical model and field conditions, we inverted simulated data for the best performing hydrological modeling parameters and measured data (transfer resistances). Peaks in PDF curves indicate that the α values for the SSF and WMF are 0.018 and 0.016 m^{-1}, respectively, and likewise n values are 1.24 and 1.91. Figure 9 shows an inverted model from the real data and a corresponding model from data simulated with the stated hydrological parameters. There is a strong correlation between simulated and measured transfer resistances (Figure 9a), with a Pearson correlation coefficient of 0.88.

5. Discussion

5.1. Synthetic Case Study

The McMC chains encountered the part of the parameter space with the maximum likelihood corresponding to the known values in the synthetic case for α and n. Modal model values correspond to a normalized likelihood value of ∼0.7, which is relatively high as the theoretical maximum value is 1 (and can only be achieved when the sum of residuals is equal to 0). Parameter densities are high close to the known parameters of the synthetic case study; for example, the mean n parameter for the sandstone formation is 1.99 ± 0.37, while the known value is 1.90. Normality tests of the McMC samples indicate normality, having a Shapiro-Wilk statistic of ≥0.9. However, the resulting distributions are multimodal and there is an apparent insensitivity to K; therefore, mean and standard deviation statistics do not fully capture the nature of the coupled modeling results. However, peaks in PDF curves compare favorably to known n values, but in the case of the α parameter it is difficult to quantify the uncertainty due to sampling in log space (and spanning an order of magnitude) but it does overlap with the known α.

Generally, other studies have found that synthetic case studies perform well, due to the hydrological model being well realized (Hinnell et al., 2010; Pleasants et al., 2022). Conversely, the synthetic data errors are simulated at only 2% and synthetic modeling does not indicate how well the approach will perform when aspects of the hydrological modeling are more uncertain (as in the field case). There are two further discussion points regarding the coupled modeling shown here that deserve attention. First, several (12) Markov chains were required to explore the parameter space appropriately. Second, the coupled modeling for this problem shows relative weak sensitivity to hydraulic conductivity (K). This is likely due to this study having most sensitivity to the unsaturated near surface where the α and n parameters of van Genuchten are a dominant control on saturation and, by

19447973, 2024, 10, Downloaded from https://agupubs.onlinelibrary.wiley.com/doi/10.1029/2023WR036319 by British Geological Survey, Wiley Online Library on [04/12/2024]. See the Terms and Conditions (https://onlinelibrary.wiley.com/terms-and-conditions) on Wiley Online Library for rules of use; OA articles are governed by the applicable Creative Commons License

10.1029/2023WR036319

19447973, 2024, 10, Downloaded from https://agupubs.onlinelibrary.wiley.com/doi/10.1029/2023WR036319 by British Geological Survey, Wiley Online Library on [04/12/2024]. See the Terms and Conditions (https://onlinelibrary.wiley.com/terms-and-conditions) on Wiley Online Library for rules of use; OA articles are governed by the applicable Creative Commons License

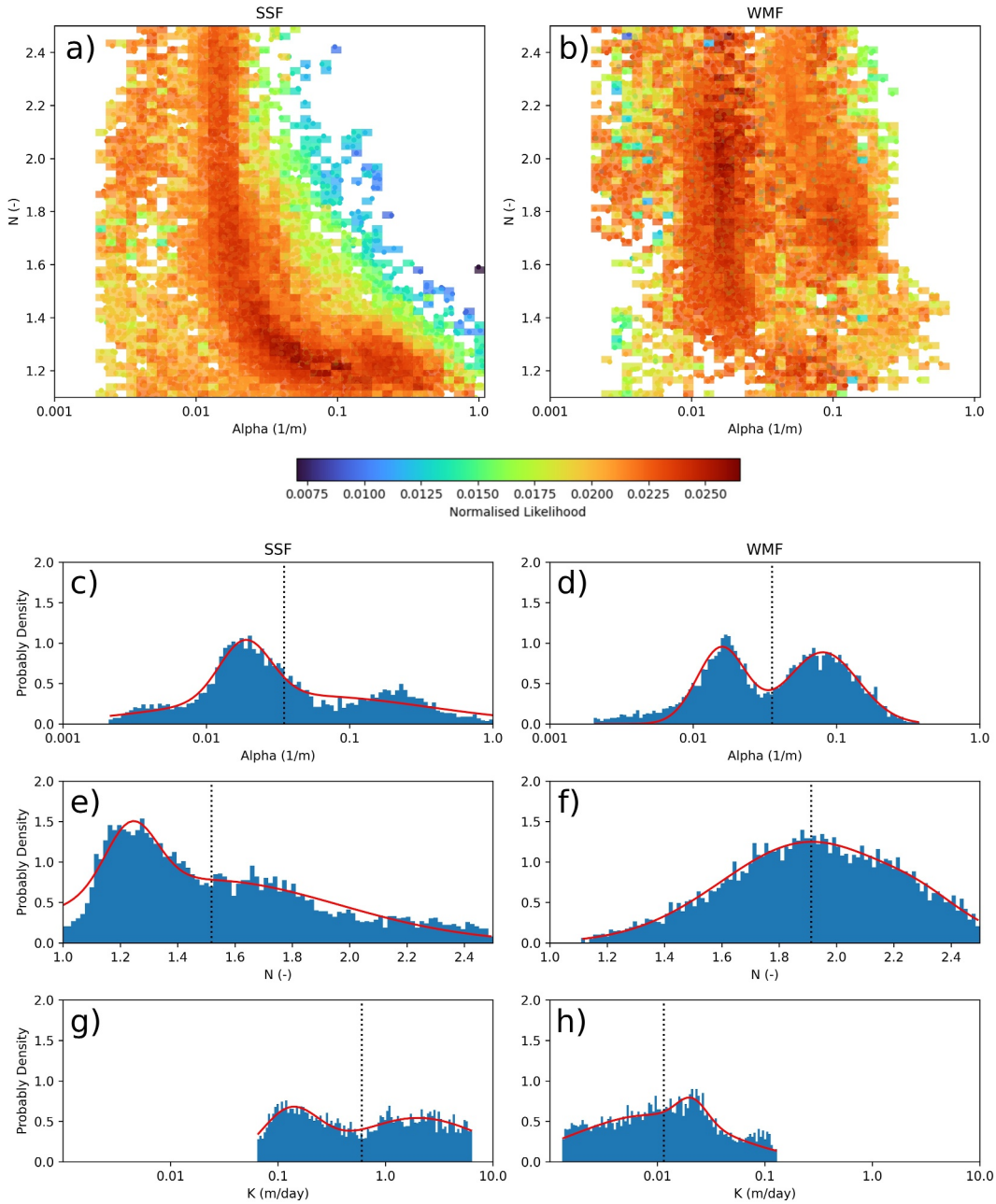

Figure 7. Results of Markov chain Monte Carlo (McMC) chains for the field case study showing the intensity and likelihood values for (a) the Staithes Sandstone Formation (SSF) and (b) the Whitby Mudstone Formation (WMF). Plots (c)–(h) show the probability density histograms of the 6 fitted parameters. Red lines show the PDFs which are a mix of Gaussian and bimodal curves. Black dashed lines indicate the means of the McMC parameter samples.

Table 6
Results of Finding Mean and Standard Deviations for the Sampled Parameters Shown in Figure 7

Unit	$\log_{10}(K$ (m. day^{-1}))	$W(K)$	$\log_{10}(\alpha$ (m^{-1}))	$W(\alpha)$	n (–)	$W(n)$
SSF	−0.22 ± 0.58	0.95	−1.46 ± 0.58	0.98	1.52 ± 0.37	0.94
WMF	−1.93 ± 0.50	0.97	−1.45 ± 0.46	0.98	1.91 ± 0.29	0.99

Note. W refers to the normality statistic according to Shapiro and Wilk (1965) for K, α, and n respectively. The sample size is 7,003.

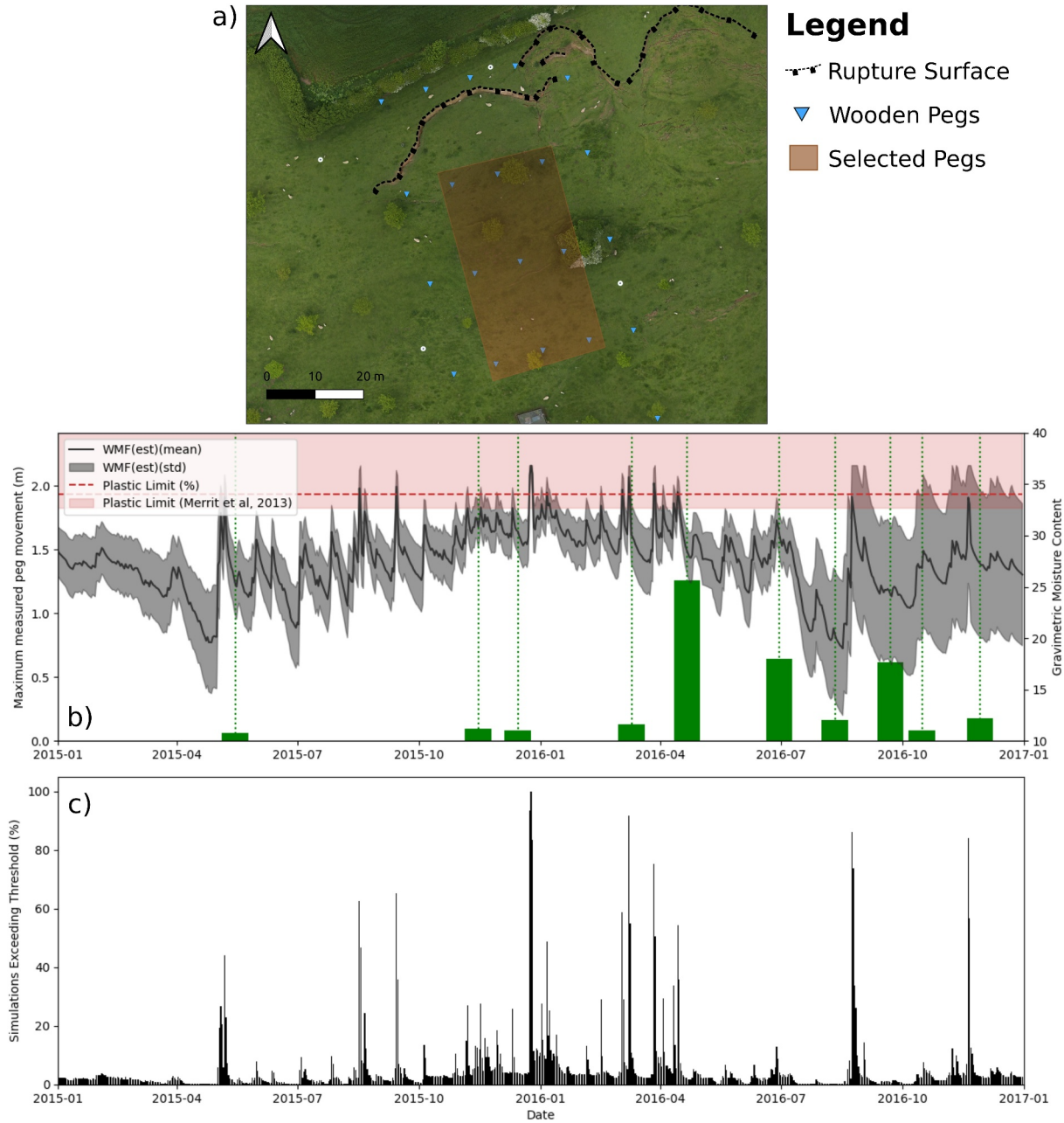

Figure 8. (a) Plan view showing an aerial image of the backscarp at Hollin Hill that developed in the spring of 2016 (Peppa et al., 2019). The box shows the location of monitoring pegs downslope of the backscarp, used here to quantify slope movements. (b) Time series shows gravimetric moisture content estimate in the sampled Whitby Mudstone Formation (WMF) (see Figure 6) and plastic limits found as part of this study and a prior study of Hollin Hill (Merritt et al., 2013). (c) Percentage of simulations exceeding the plastic limit for a given date.

extension, resistivity. It should be noted that unsaturated pore pressures, as well as saturation, also depend on hydraulic conductivity, but the coupled modeling in this study is less sensitive to this parameter. Other studies have shown that coupled approaches can be sensitive to hydraulic conductivity on slopes (Pleasants et al., 2022), and therefore the sensitivity to K could be helped by fixing other parameters like α and n in the McMC sampling.

5.2. Field Case Study

For the field case, the McMC chains appear to converge on a discrete parts of the parameter space. It should be noted that the parameter space is constrained by model stability, which restricts models into a certain part of the

19447973, 2024, 10, Downloaded from https://agupubs.onlinelibrary.wiley.com/doi/10.1029/2023WR036319 by British Geological Survey, Wiley Online Library on [04/12/2024]. See the Terms and Conditions (https://onlinelibrary.wiley.com/terms-and-conditions) on Wiley Online Library for rules of use; OA articles are governed by the applicable Creative Commons License

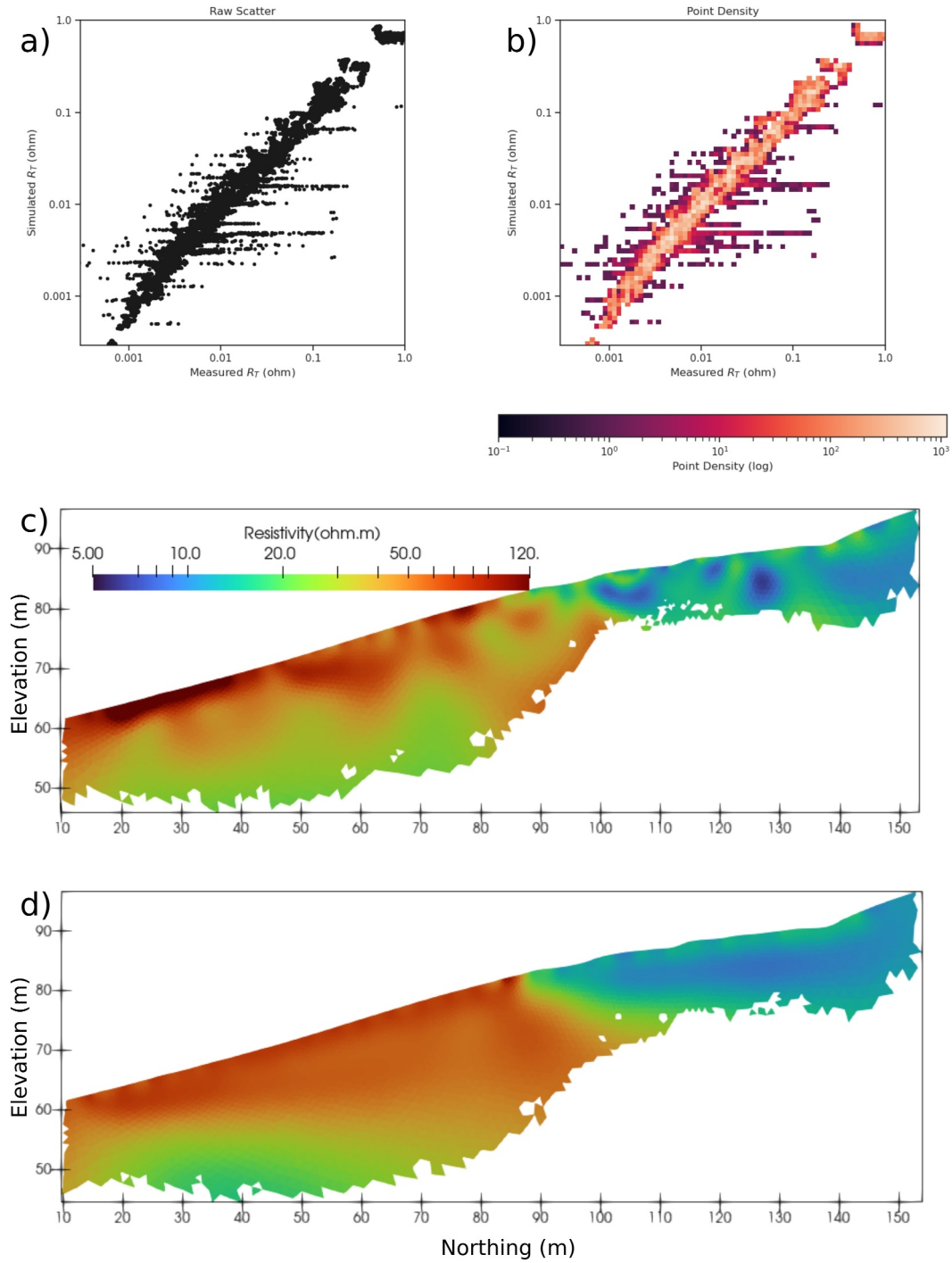

Figure 9. (a) Simulated versus measured transfer resistances (log scale) and (b) point density. Inverted sections of (c) measured transfer resistances (field data) and (d) simulated transfer resistances from hydrogeophysical modeling. Both measured and simulated sets relate to April 2015. The lower part of the model has been masked by the relative sensitivity of the electrical resistivity tomography solution.

parameter space even without McMC sampling. The modal/dominant values correspond to a likelihood value of ~0.026, which is over an order of magnitude smaller than that used in the synthetic modeling. We anticipated that the field results would be challenging to optimize, as other recent studies suggest, field data and (particularly hydrological) models have greater uncertainties associated with them compared to synthetic studies (Pleasants

19447973, 2024, 10, Downloaded from https://agupubs.onlinelibrary.wiley.com/doi/10.1029/2023WR036319 by British Geological Survey, Wiley Online Library on [04/12/2024]. See the Terms and Conditions (https://onlinelibrary.wiley.com/terms-and-conditions) on Wiley Online Library for rules of use; OA articles are governed by the applicable Creative Commons License

19447973, 2024, 10, Downloaded from https://agupubs.onlinelibrary.wiley.com/doi/10.1029/2023WR036319 by British Geological Survey, Wiley Online Library on [04/12/2024]. See the Terms and Conditions (https://onlinelibrary.wiley.com/terms-and-conditions) on Wiley Online Library for rules of use; OA articles are governed by the applicable Creative Commons License

et al., 2022; Tso et al., 2020). Data errors are relatively small (reciprocal measurements suggest that most are <5%) and the assessment of forward modeling errors in the geophysical simulator (R2) is easy to assess. However, the potential for high modeling errors in SUTRA is significant and difficult to fully quantify. The realism in the hydrological model is uncertain, but as Linde et al. (2015) remark, the value in hydrogeophysical modeling is to better inform any conclusions or decisions under uncertainty. As with the synthetic case we find distributions with more than one modal value (Figure 7). Although Shapiro-Wilk tests strongly suggest that the samples are normal; as with the synthetic case, mean and standard deviation statistics do not capture the full details of the McMC sampling. Peaks can be observed in the resulting PDF analysis of McMC samples that do not correspond to the mean. Once more, hydraulic conductivity is drawn from a prior distribution an order of magnitude above and below empirically found values, but the McMC sampling is unable to further constrain this distribution for reasons cited in the discussion about the synthetic case.

Generated apparent resistivity pseudosections simulated by the modal hydrological model and those measured at the field site are comparable (Figure S2 in Supporting Information S1), which is promising as it shows the geometry and magnitude of the resulting resistivity distributions from hydrological models are representative. Additionally, we inverted simulated data from the hydrogeophysical modeling and measured data, the resulting modeling responses are similar (Figure 9). Comparing the results to laboratory-derived n and α values shows there is overlap, although the range of possible n parameters predicted by the hydrogeophysical modeling is large, PDF curves suggest that the n parameter derived from coupled modeling, is 1.91 ± 0.31 which overlaps with the value of predicted by curve fitting (1.61 ± 0.11). The α parameter predicted by curve fitting is 0.040 ± 0.030 m^{-1}, whereas hydrogeophysical modeling predicts the most likely α values (once anti-logged) to be 0.016 and 0.080 m^{-1}, with a mean value of 0.035 m^{-1}. Therefore, the coupled modeling has constrained the unsaturated soil retention parameters.

5.2.1. Further Modeling

For each timestep in the hydrological model we computed an average saturation for a sample point in the WMF (Figure 6) and a standard deviation. It is possible to visualize a range of saturations present on the slope for multiple hydrological model realizations with differing soil-water retention parameters over time (Figure 8b). It was not possible to additionally simulate the role of hydraulic conductivity on these models as PDFs could not be reliably generated from the McMC samples. We observe that saturation values of the near-surface WMF and SSF respond to rainfall events and evapotranspiration as high frequency events. High frequency responses to rainfall are replicated in VWC measurements made by the COSMOS station at Hollin Hill which indicates that the saturation changes modeled by SUTRA are reflective of reality. We computed a Pearson correlation coefficient of 0.6 between the modeled saturation values for the WMF and COSMOS VWC measurements; this shows moderate correlation. Notably several peaks in saturation are not as apparent in the year prior to the movement (2015), whilst the sustained high saturation in the WMF at Hollin Hill in the late winter/early spring of 2015/2016 proceeds the development of a rotational failure (Figure 8). This suggests that these higher saturation (or GMC) values reduced shear strength in the slope and encouraged movement. Indeed, peaks in GMC can be observed prior to recorded movements (Figure 8).

We argue that the hydrological model, calibrated with geophysical measurements, provides context for the slope movements observed at Hollin Hill and could be conceivably expanded to calibrate a coupled hydro-geomechanical model (as modeled saturation levels in the near surface are sensitive to the van Genuchten soil retention parameters).

5.3. Limitations and Scope

Multimodal distributions are apparent for the unsaturated soil retention parameters, nevertheless, likely values for these parameters have been further constrained by the coupled modeling over their respective prior PDFs. Regarding the bimodal nature of the α parameter distribution in the WMF (Figure 7d), the permeability of this formation is relatively low compared to the SSF. In field monitoring suggests that the WMF remains at a relatively high moisture content throughout seasonal cycles and therefore wetting fronts are muted in the resistivity sections. Hence the geophysical signal against which the coupled modeling can be calibrated is limited. The calibration would be more reliable in a scenario where the formation experiences a wider range of saturations; nevertheless,

19447973, 2024, 10, Downloaded from https://agupubs.onlinelibrary.wiley.com/doi/10.1029/2023WR036319 by British Geological Survey, Wiley Online Library on [04/12/2024]. See the Terms and Conditions (https://onlinelibrary.wiley.com/terms-and-conditions) on Wiley Online Library for rules of use; OA articles are governed by the applicable Creative Commons License

decreases in resistivity are observed in the shallow WMF over years related to rainfall events (Boyd et al., 2021; Uhlemann et al., 2017) and the apparent agreement with laboratory-derived values is promising.

With the field array setup being a surface arrangement of electrodes, the sensitivity of the array is constrained to the near surface where the subsurface is likely to be unsaturated, and where the α and n parameters play a dominant role in modeling saturation levels within SUTRA. Moreover, a saturated formation will have other factors driving changes in its resistivity, namely pore fluid conductivity and temperature. In saturated conditions tracer injection tests coupled with resistivity monitoring would be a more appropriate input for hydrogeophysical models (e.g., Tso et al., 2020). That said, our ultimate aim, which has been achieved, is to derive a posteriori distributions of hydraulic parameters that can be used to aid slope stability modeling.

Tso et al. (2019) highlight that errors in the petrophysical calibration of geoelectrical data can have profound effects on moisture content estimates. Hollin Hill is a heterogeneous environment and therefore spatial discrepancies in the petrophysical relationship are likely, particularly regarding porosity (which in part is why we avoid fitting a petrophysical relationship where porosity is a key parameter). Moreover, the formations of Hollin Hill exhibit some degree of anisotropy (Figure 2) that additionally makes petrophysical calibration require appreciation of electrical current flow orientation, though anisotropic current solutions exist (e.g., Herwanger et al., 2004) they are not implemented here.

We have assumed that the samples analyzed are representative, and their temperature correction is accurate. Uncertainties in the petrophysical transfer function, real world geometrical boundaries and heterogeneity are likely to contribute to modeling errors. Moreover, shrink swell processes on Hollin Hill merit some further discussion. At the macro scale shrink-swell processes and slope movements result in tension cracks; this would account for the apparent reduction in volume in the material at lower moisture contents. Cracks would invariably increase local hydraulic conductivity, effective porosity, and electrical resistivity (Bièvre et al., 2012); as such they pose a challenge regardless of whether one attempts geophysical or hydrological modeling. Modeling such mechanics is not possible with SUTRA 3.0 without significant modification that is beyond the goals of this paper, but formulations of unsaturated flow in media with a variable porosity do exist (e.g., Camporese et al., 2006). On the other hand, cracking is only present in the near-surface of the WMF (Peppa et al., 2019), and we attempt to account for the higher resistivity of near surface WMF in this study with its own petrophysical relationship. In addition to cracking, Hollin Hill is subject to slope movements. In this study it is assumed that slope movements over the 2-year monitoring period are inconsequential to the geophysical or hydrological modeling. Over longer periods of time, however, accounting for the placement of geophysical sensors and topography is important for accurate geophysical modeling (Boyd et al., 2021; Whiteley et al., 2020) and would therefore need considering if attempting to model parameters for a longer time period. Regarding hydrological modeling, changing the external geometry of the modeling domain during simulations is not possible with SUTRA 3.0, hence assuming topography is invariable is a necessity.

In this study the modeling domain was restricted to 2D due to its relative simplicity to define formation boundaries and significantly reduced computation time versus modeling in 3D (which would require significantly more elements in the modeling domain). Conversely 2D geoelectrical models (of Hollin Hill), for example, compare favorably to their 3D counterparts as the slope features are prominently orientated parallel to the strike of the slope. But Hollin Hill is an inherently 3D environment, so future work should include 3D hydrogeophysical modeling efforts that capture electrical and unsaturated fluid flow in four dimensions. With that said, the McMC method can be prohibitive regarding computation time; we ran our 2D scenario on a dual processor system (two Intel Xeon E5-2637V3) initially for testing our parallel Python code and it took several weeks to complete. We opted to use relatively modern computing hardware for our production runs, which improved our run times; hence it is inevitable that as computer processors and resources become more efficient, the time required for running coupled hydrogeophysical models (even in 3D) will become more tenable.

6. Conclusion

We tested the feasibility of our coupled geophysical and hydrological modeling via an McMC algorithm for a synthetic case study, where all relevant modeling parameters are known for a two-layer system. We found that the McMC chains are sensitive to the van Genuchten n and α parameters, given that the highest likelihood values observed in the parameter space correspond to the known values of n and α. However, the McMC sampling is apparently insensitive to hydraulic conductivity in this case, and therefore the coupled approach presented here

cannot be used to constrain this parameter. Furthermore, resulting parameter distributions can be multimodal, hence simple fitting statistics like mean and standard deviation do not fully capture the information the McMC samples provide.

Regarding the field case Hollin Hill landslide site, McMC chains maximize likelihood reasonably well (as found in the synthetic case). Tests of normality suggest the parameter distributions are largely normal, but distributions of results are skewed toward modal values. Conversely, the maximum normalized likelihood value for the modal soil retention parameters (found from the posterior PDFs) is an order of magnitude lower than in the synthetic case; we attribute this to significant modeling errors in the hydrological model that are hard to quantify. There are other limitations, such as our assumption that the petrophysical relationships, seasonal temperature models and 2D modeling domain are adequate for our purposes. Furthermore, as with the synthetic case study the McMC sampling was unable to constrain hydraulic conductivity values.

Nevertheless, we contend that the coupled hydrogeophysical model is sensitive to soil retention parameters for measurements made at Hollin Hill and have been able to assign PDFs which describe a range of possible α and n parameters for the mudstone and sandstone formations. We find promising overlap with van Genuchten parameters determined through conventional curve fitting for the WMF. Monte-Carlo simulations imply that high soil moisture contents were maintained in the near-surface WMF (the actively failing unit) prior to an observed rotational failure, this occurred in 100% of simulations and the GMC of the material apparently exceeded its plastic limit. Furthermore, we find that the calibrated hydrological modeling simulated several instances of elevated moisture contents prior to other slope movements. This work demonstrates hydrogeophysical modeling can be used to generate hydromechanical models for several parameter combinations. We therefore suggest that future studies could incorporate geophysical measurements as a means to understand uncertainties in slope stability models under various scenarios in landslide monitoring and early warning systems.

Data Availability Statement

The rainfall (and evapotranspiration) data on which parts of this manuscript are based, are derived from the (open access) COSMOS-UK data set for the years between 2013 and 2017, see Stanley et al. (2019). The topography of the field site is derived from laser ranging and drone studies (Boyd et al., 2021; Peppa et al., 2019). The code, and data, required to complete the work shown in this manuscript have been added to a Github repository (Boyd, 2023a), likewise modified version of SUTRA 3.0 can also be found on Github (Boyd, 2023b).

Acknowledgments
We would like to thank Josie Gibson, Frances Standen, and James Standen for their continued support over the years of monitoring Hollin Hill. This work is supported by the NERC Doctoral Training Program ENVISION (NE/L002604/1) and is published with the permission of the Executive Director of the British Geological Survey (NERC). We would also like to thank the associate editor (Sander Huisman) and three anonymous reviewers for their valuable input for improving the quality of the manuscript.

References

Allen, R. G., Pereira, L. S., Raes, D., & Smith, M. (1998). *Crop evapotranspiration-Guidelines for computing crop water requirements-FAO Irrigation and drainage paper 56* (Vol. 300, No. (9), p. D05109). FAO.

Allen, R. G., Pruitt, W. O., Wright, J. L., Howell, T. A., Ventura, F., Snyder, R., et al. (2006). A recommendation on standardized surface resistance for hourly calculation of reference ET_o by the FAO56 Penman-Monteith method. *Agricultural Water Management*, *81*(1), 1–22. https://doi.org/10.1016/j.agwat.2005.03.007

Archie, G. E. (1942). The electrical resistivity log as an aid in determining some reservoir characteristics. *Transactions of the AIME*, *146*(01), 54–62. https://doi.org/10.2118/942054-g

Archie, G. E. (1947). Electrical resistivity an aid in core-analysis interpretation. *AAPG Bulletin*, *31*(2), 350–366. https://doi.org/10.1306/3d93395c-16b1-11d7-8645000102c1865d

Bichler, A., Bobrowsky, P., Best, M., Douma, M., Hunter, J., Calvert, T., & Burns, R. (2004). Three-dimensional mapping of a landslide using a multi-geophysical approach: The Quesnel Forks landslide. *Landslides*, *1*(1), 29–40. https://doi.org/10.1007/s10346-003-0008-7

Bièvre, G., Jongmans, D., Winiarski, T., & Zumbo, V. (2012). Application of geophysical measurements for assessing the role of fissures in water infiltration within a clay landslide (Trièves area, French Alps). *Hydrological Processes*, *26*(14), 2128–2142. https://doi.org/10.1002/hyp.7986

Binley, A., Cassiani, G., Middleton, R., & Winship, P. (2002). Vadose zone flow model parameterisation using cross-borehole radar and resistivity imaging. *Journal of Hydrology*, *267*(3), 147–159. https://doi.org/10.1016/S0022-1694(02)00146-4

Binley, A., & Slater, L. (2020). *Resistivity and induced polarization: Theory and applications to the near-surface Earth*. Cambridge University Press.

Bishop, A. W. (1959). The principle of effective stress. *Teknisk Ukeblad*, *39*, 859–863.

Blanchy, G., Saneiyan, S., Boyd, J., McLachlan, P., & Binley, A. (2019). ResIPy, an intuitive open source software for complex geoelectrical inversion/modeling in 2D space.

Boyd, J. P. (2023a). HHcoupled. [Software]. https://doi.org/10.5281/zenodo.10797144

Boyd, J. P. (2023b). Modified version SUTRA 3.0. [Software]. https://doi.org/10.5281/zenodo.10797153

Boyd, J. P., Binley, A., Wilkinson, P., Holmes, J., Bruce, E., & Chambers, J. (2024). Practical considerations for using petrophysics and geoelectrical methods on clay rich landslides. *Engineering Geology*, *334*, 107506. https://doi.org/10.1016/j.enggeo.2024.107506

Boyd, J. P., Chambers, J., Wilkinson, P., Peppa, M., Watlet, A., Kirkham, M., et al. (2021). A linked geomorphological and geophysical modelling methodology applied to an active landslide. *Landslides*, *18*(8), 1–16. https://doi.org/10.1007/s10346-021-01666-w

Brunet, P., Clément, R., & Bouvier, C. (2010). Monitoring soil water content and deficit using Electrical Resistivity Tomography (ERT) – A case study in the Cevennes area, France. *Journal of Hydrology*, *380*(1), 146–153. https://doi.org/10.1016/j.jhydrol.2009.10.032

19447973, 2024, 10, Downloaded from https://agupubs.onlinelibrary.wiley.com/doi/10.1029/2023WR036319 by British Geological Survey, Wiley Online Library on [04/12/2024]. See the Terms and Conditions (https://onlinelibrary.wiley.com/terms-and-conditions) on Wiley Online Library for rules of use; OA articles are governed by the applicable Creative Commons License

Camporese, M., Cassiani, G., Deiana, R., Salandin, P., & Binley, A. (2015). Coupled and uncoupled hydrogeophysical inversions using ensemble Kalman filter assimilation of ERT-monitored tracer test data. *Water Resources Research*, *51*(5), 3277–3291. https://doi.org/10.1002/2014WR016017

Camporese, M., Ferraris, S., Putti, M., Salandin, P., & Teatini, P. (2006). Hydrological modeling in swelling/shrinking peat soils. *Water Resources Research*, *42*(6), W06420. https://doi.org/10.1029/2005WR004495

Cardoso, R., & Dias, A. S. (2017). Study of the electrical resistivity of compacted kaolin based on water potential. *Engineering Geology*, *226*, 1–11. https://doi.org/10.1016/j.enggeo.2017.04.007

Carey, A. M., Paige, G. B., Carr, B. J., & Dogan, M. (2017). Forward modeling to investigate inversion artifacts resulting from time-lapse electrical resistivity tomography during rainfall simulations. *Journal of Applied Geophysics*, *145*, 39–49. https://doi.org/10.1016/j.jappgeo.2017.08.002

Chambers, J. E., Wilkinson, P. B., Kuras, O., Ford, J. R., Gunn, D. A., Meldrum, P. I., et al. (2011). Three-dimensional geophysical anatomy of an active landslide in Lias Group mudrocks, Cleveland Basin, UK. *Geomorphology*, *125*(4), 472–484. https://doi.org/10.1016/j.geomorph.2010.09.017

Crawford, M. M., & Bryson, L. S. (2018). Assessment of active landslides using field electrical measurements. *Engineering Geology*, *233*, 146–159. https://doi.org/10.1016/j.enggeo.2017.11.012

De Vita, P., Di Maio, R., & Piegari, E. (2012). A study of the correlation between electrical resistivity and matric suction for unsaturated ash-fall pyroclastic soils in the Campania region (southern Italy). *Environmental Earth Sciences*, *67*(3), 787–798. https://doi.org/10.1007/s12665-012-1531-4

Duncan, J. M., Wright, S. G., & Brandon, T. L. (2014). *Soil strength and slope stability* (2nd ed.). John Wiley & Sons.

Fischer, E. M., & Knutti, R. (2016). Observed heavy precipitation increase confirms theory and early models. *Nature Climate Change*, *6*(11), 986–991. https://doi.org/10.1038/nclimate3110

François, B., Tacher, L., Bonnard, C., Laloui, L., & Triguero, V. (2007). Numerical modelling of the hydrogeological and geomechanical behaviour of a large slope movement: The Triesenberg landslide (Liechtenstein). *Canadian Geotechnical Journal*, *44*(7), 840–857. https://doi.org/10.1139/t07-028

Fredlund, D. G., Morgenstern, N. R., & Widger, R. (1978). The shear strength of unsaturated soils. *Canadian Geotechnical Journal*, *15*(3), 313–321. https://doi.org/10.1139/t78-029

Fredlund, D. G., Xing, A., Fredlund, M. D., & Barbour, S. (1996). The relationship of the unsaturated soil shear to the soil-water characteristic curve. *Canadian Geotechnical Journal*, *33*(3), 440–448. https://doi.org/10.1139/t96-065

Galavi, V. (2010). Groundwater flow, fully coupled flow deformation and undrained analyses in PLAXIS 2D and 3D.

Gelman, A., Gilks, W. R., & Roberts, G. O. (1997). Weak convergence and optimal scaling of random walk Metropolis algorithms. *Annals of Applied Probability*, *7*(1), 110–120. https://doi.org/10.1214/aoap/1034625254

Gibson, A. D., Culshaw, M. G., Dashwood, C., & Pennington, C. V. L. (2013). Landslide management in the UK—The problem of managing hazards in a 'low-risk' environment. *Landslides*, *10*(5), 599–610. https://doi.org/10.1007/s10346-012-0346-4

Glover, P. W., Hole, M. J., & Pous, J. (2000). A modified Archie's law for two conducting phases. *Earth and Planetary Science Letters*, *180*(3), 369–383. https://doi.org/10.1016/s0012-821x(00)00168-0

Gunn, D., Chambers, J., Hobbs, P., Ford, J., Wilkinson, P., Jenkins, G., & Merritt, A. (2013). Rapid observations to guide the design of systems for long-term monitoring of a complex landslide in the Upper Lias clays of North Yorkshire, UK. *Quarterly Journal of Engineering Geology and Hydrogeology*, *46*(3), 323–336. https://doi.org/10.1144/qjegh2011-028

Hastings, W. K. (1970). Monte Carlo sampling methods using Markov chains and their applications. *Biometrika*, *57*(1), 97–109. https://doi.org/10.1093/biomet/57.1.97

Hayley, K., Bentley, L. R., Gharibi, M., & Nightingale, M. (2007). Low temperature dependence of electrical resistivity: Implications for near surface geophysical monitoring. *Geophysical Research Letters*, *34*(18), L18402. https://doi.org/10.1029/2007GL031124

Herwanger, J. V., Pain, C. C., Binley, A., De Oliveira, C. R. E., & Worthington, M. H. (2004). Anisotropic resistivity tomography. *Geophysical Journal International*, *158*(2), 409–425. https://doi.org/10.1111/j.1365-246X.2004.02314.x

Hinnell, A. C., Ferré, T. P. A., Vrugt, J. A., Huisman, J. A., Moysey, S., Rings, J., & Kowalsky, M. B. (2010). Improved extraction of hydrologic information from geophysical data through coupled hydrogeophysical inversion. *Water Resources Research*, *46*(4), W00D40. https://doi.org/10.1029/2008WR007060

Hobbs, P., Entwisle, D., Northmore, K., Sumbler, M., Jones, L., Kemp, S., et al. (2005). The Engineering Geology of UK rocks and soils: The Lias Group. British Geological Survey IR/05/008, Nottingham, UK.

Hobbs, P., Jones, L., Roberts, P., & Haslam, E. (2010). SHRINKiT: Automated measurement of shrinkage limit for clay soils.

Holmes, J., Chambers, J., Meldrum, P., Wilkinson, P., Boyd, J., Williamson, P., et al. (2020). Four-dimensional electrical resistivity tomography for continuous, near-real-time monitoring of a landslide affecting transport infrastructure in British Columbia, Canada. *Near Surface Geophysics*, *18*(Geoelectrical Monitoring), 337–351. https://doi.org/10.1002/nsg.12102

Holmes, J., Chambers, J., Wilkinson, P., Meldrum, P., Cimpoiaşu, M., Boyd, J., et al. (2022). Application of petrophysical relationships to electrical resistivity models for assessing the stability of a landslide in British Columbia, Canada. *Engineering Geology*, *301*, 106613. https://doi.org/10.1016/j.enggeo.2022.106613

Johnson, T. C., Versteeg, R. J., Ward, A., Day-Lewis, F. D., & Revil, A. (2010). Improved hydrogeophysical characterization and monitoring through parallel modeling and inversion of time-domain resistivity and induced-polarization data. *Geophysics*, *75*(4), WA27–WA41. https://doi.org/10.1190/1.3475513

Kuras, O., Pritchard, J. D., Meldrum, P. I., Chambers, J. E., Wilkinson, P. B., Ogilvy, R. D., & Wealthall, G. P. (2009). Monitoring hydraulic processes with automated time-lapse electrical resistivity tomography (ALERT). *Comptes Rendus Geoscience*, *341*(10), 868–885. https://doi.org/10.1016/j.crte.2009.07.010

Linde, N., Renard, P., Mukerji, T., & Caers, J. (2015). Geological realism in hydrogeological and geophysical inverse modeling: A review. *Advances in Water Resources*, *86*, 86–101. https://doi.org/10.1016/j.advwatres.2015.09.019

Loke, M. H., Chambers, J. E., Rucker, D. F., Kuras, O., & Wilkinson, P. B. (2013). Recent developments in the direct-current geoelectrical imaging method. *Journal of Applied Geophysics*, *95*(Supplement C), 135–156. https://doi.org/10.1016/j.jappgeo.2013.02.017

Lu, N., & Godt, J. (2008). Infinite slope stability under steady unsaturated seepage conditions. *Water Resources Research*, *44*(11), n/a. https://doi.org/10.1029/2008WR006976

Lu, N., & Likos, W. J. (2006). Suction stress characteristic curve for unsaturated soil. *Journal of Geotechnical and Geoenvironmental Engineering*, *132*(2), 131–142. https://doi.org/10.1061/(ASCE)1090-0241(2006)132:2(131)

Ma, R., McBratney, A., Whelan, B., Minasny, B., & Short, M. (2011). Comparing temperature correction models for soil electrical conductivity measurement. *Precision Agriculture*, *12*(1), 55–66. https://doi.org/10.1007/s11119-009-9156-7

19447973, 2024, 10, Downloaded from https://agupubs.onlinelibrary.wiley.com/doi/10.1029/2023WR036319 by British Geological Survey, Wiley Online Library on [04/12/2024]. See the Terms and Conditions (https://onlinelibrary.wiley.com/terms-and-conditions) on Wiley Online Library for rules of use; OA articles are governed by the applicable Creative Commons License

Mboh, C. M., Huisman, J. A., Van Gaelen, N., Rings, J., & Vereecken, H. (2012). Coupled hydrogeophysical inversion of electrical resistances and inflow measurements for topsoil hydraulic properties under constant head infiltration. *Near Surface Geophysics*, *10*(5), 413–426. https://doi.org/10.3997/1873-0604.2012009

Merritt, A. J., Chambers, J. E., Murphy, W., Wilkinson, P. B., West, L. J., Gunn, D. A., et al. (2013). 3D ground model development for an active landslide in Lias mudrocks using geophysical, remote sensing and geotechnical methods. *Landslides*, *11*(4), 537–550. https://doi.org/10.1007/s10346-013-0409-1

Merritt, A. J., Chambers, J. E., Murphy, W., Wilkinson, P. B., West, L. J., Uhlemann, S., et al. (2018). Landslide activation behaviour illuminated by electrical resistance monitoring. *Earth Surface Processes and Landforms*, *43*(6), 1321–1334. https://doi.org/10.1002/esp.4316

Merritt, A. J., Chambers, J. E., Wilkinson, P. B., West, L. J., Murphy, W., Gunn, D., & Uhlemann, S. (2016). Measurement and modelling of moisture—Electrical resistivity relationship of fine-grained unsaturated soils and electrical anisotropy. *Journal of Applied Geophysics*, *124*(Supplement C), 155–165. https://doi.org/10.1016/j.jappgeo.2015.11.005

METER Group Inc. Hyprop 2: Soil moisture release curves. Retrieved from https://www.metergroup.com/en/meter-environment/products/hyprop-2-soil-moisture-release-curves

Montaron, B. (2009). Connectivity theory – A new approach to modeling non-Archie rocks. *Petrophysics - The SPWLA Journal of Formation Evaluation and Reservoir Description*, *50*(02), 102–115.

Moradi, S., Heinze, T., Budler, J., Gunatilake, T., Kemna, A., & Huisman, J. A. (2021). Combining site characterization, monitoring and hydromechanical modeling for assessing slope stability. *Land*, *10*(4), 423. https://doi.org/10.3390/land10040423

Ogilvy, R., Meldrum, P., Kuras, O., Wilkinson, P., Chambers, J., Sen, M., et al. (2009). Automated monitoring of coastal aquifers with electrical resistivity tomography. *Near Surface Geophysics*, *7*(5–6), 367–376. https://doi.org/10.3997/1873-0604.2009027

Pazzi, V., Morelli, S., & Fanti, R. (2019). A review of the advantages and limitations of geophysical investigations in landslide studies. *International Journal of Geophysics*, *2019*, 2983087. https://doi.org/10.1155/2019/2983087

Peppa, M. V., Mills, J. P., Moore, P., Miller, P. E., & Chambers, J. E. (2019). Automated co-registration and calibration in SfM photogrammetry for landslide change detection. *Earth Surface Processes and Landforms*, *44*(1), 287–303. https://doi.org/10.1002/esp.4502

Perrone, A., Lapenna, V., & Piscitelli, S. (2014). Electrical resistivity tomography technique for landslide investigation: A review. *Earth-Science Reviews*, *135*, 65–82. https://doi.org/10.1016/j.earscirev.2014.04.002

Pleasants, M. S., Neves, F. D. A., Parsekian, A. D., Befus, K. M., & Kelleners, T. J. (2022). Hydrogeophysical inversion of time-lapse ERT data to determine hillslope subsurface hydraulic properties. *Water Resources Research*, *58*(4), e2021WR031073. https://doi.org/10.1029/2021WR031073

Provost, A. M., & Voss, C. I. (2019). SUTRA, a model for saturated-unsaturated, variable-density groundwater flow with solute or energy transport—Documentation of generalized boundary conditions, a modified implementation of specified pressures and concentrations or temperatures, and the lake capability. (6-A52). Retrieved from http://pubs.er.usgs.gov/publication/tm6A52

Razali, N. M., & Wah, Y. B. (2011). Power comparisons of Shapiro-Wilk, Kolmogorov-Smirnov, Lilliefors and Anderson-Darling tests. *Journal of Statistical Modeling and Analytics*, *2*(1), 21–33.

Roberts, G. O., & Rosenthal, J. S. (2001). Optimal scaling for various Metropolis-Hastings algorithms. *Statistical Science*, *16*(4), 351–367. https://doi.org/10.1214/ss/1015346320

Shah, P. H., & Singh, D. (2005). Generalized Archie's law for estimation of soil electrical conductivity. *Journal of ASTM International*, *2*(5), 1–20. https://doi.org/10.1520/jai13087

Shapiro, S. S., & Wilk, M. B. (1965). An analysis of variance test for normality (complete samples). *Biometrika*, *52*(3/4), 591–611. https://doi.org/10.2307/2333709

Stanley, S., Antoniou, V., Ball, L. A., Bennett, E. S., Blake, J. R., Boorman, D. B., et al. (2019). Daily and sub-daily hydrometeorological and soil data (2013-2017) [COSMOS-UK] [Dataset]. https://doi.org/10.5285/a6012796-291c-4fd6-a7ef-6f6ed0a6cfa5

Tacher, L., Bonnard, C., Laloui, L., & Parriaux, A. (2005). Modelling the behaviour of a large landslide with respect to hydrogeological and geomechanical parameter heterogeneity. *Landslides*, *2*(1), 3–14. https://doi.org/10.1007/s10346-004-0038-9

Terzaghi, K. V. (1936). The shearing resistance of saturated soils and the angle between the planes of shear. In *Paper presented at the Proceedings of the 1st international conference on soil mechanics and foundation engineering*.

Thakur, V. K. S., Sreedeep, S., & Singh, D. N. (2005). Parameters affecting soil-water characteristic curves of fine-grained soils. *Journal of Geotechnical and Geoenvironmental Engineering*, *131*(4), 521–524. https://doi.org/10.1061/(ASCE)1090-0241(2005)131:4(521)

Tso, C.-H. M., Johnson, T. C., Song, X., Chen, X., Kuras, O., Wilkinson, P., et al. (2020). Integrated hydrogeophysical modelling and data assimilation for geoelectrical leak detection. *Journal of Contaminant Hydrology*, *234*, 103679. https://doi.org/10.1016/j.jconhyd.2020.103679

Tso, C.-H. M., Kuras, O., & Binley, A. (2019). On the field estimation of moisture content using electrical geophysics: The impact of petrophysical model uncertainty. *Water Resources Research*, *55*(8), 7196–7211. https://doi.org/10.1029/2019WR024964

Uhlemann, S., Chambers, J., Wilkinson, P., Maurer, H., Merritt, A., Meldrum, P., et al. (2017). Four-dimensional imaging of moisture dynamics during landslide reactivation. *Journal of Geophysical Research: Earth Surface*, *122*(1), 398–418. https://doi.org/10.1002/2016JF003983

Uhlemann, S., Hagedorn, S., Dashwood, B., Maurer, H., Gunn, D., Dijkstra, T., & Chambers, J. (2016). Landslide characterization using P- and S-wave seismic refraction tomography — The importance of elastic moduli. *Journal of Applied Geophysics*, *134*(Supplement C), 64–76. https://doi.org/10.1016/j.jappgeo.2016.08.014

Uhlemann, S., Wilkinson, P. B., Chambers, J. E., Maurer, H., Merritt, A. J., Gunn, D. A., & Meldrum, P. I. (2015). Interpolation of landslide movements to improve the accuracy of 4D geoelectrical monitoring. *Journal of Applied Geophysics*, *121*(Supplement C), 93–105. https://doi.org/10.1016/j.jappgeo.2015.07.003

van Genuchten, M. T. (1980). A closed-form equation for predicting the hydraulic conductivity of unsaturated soils. *Soil Science Society of America Journal*, *44*(5), 892–898. https://doi.org/10.2136/sssaj1980.03615995004400050002x

Van Rossum, G., Drake, & Fred, L. (2009). Python 3 reference manual. *CreateSpace*.

van Woerden, J., Dijkstra, T. A., van Beek, L. P. H., & Bogaard, T. A. (2014). *The role of fissures in the hydrology and stability of the Hollin hill landslide*. (Masters). Utrecht University.

Varnes, D. J. (1978). Slope movement types and processes. *Special Report*, *176*, 11–33.

Virtanen, P., Gommers, R., Oliphant, T. E., Haberland, M., Reddy, T., Cournapeau, D., et al. (2020). SciPy 1.0: Fundamental algorithms for scientific computing in Python. *Nature Methods*, *17*(3), 261–272. https://doi.org/10.1038/s41592-019-0686-2

Waxman, M. H., & Smits, L. (1968). Electrical conductivities in oil-bearing shaly sands. *Society of Petroleum Engineers Journal*, *8*(02), 107–122. https://doi.org/10.2118/1863-a

Whiteley, J. S., Chambers, J., Uhlemann, S., Wilkinson, P., & Kendall, J. (2019). Geophysical monitoring of moisture-induced landslides: A review. *Reviews of Geophysics*, *57*(1), 106–145. https://doi.org/10.1029/2018rg000603

19447973, 2024, 10, Downloaded from https://agupubs.onlinelibrary.wiley.com/doi/10.1029/2023WR036319 by British Geological Survey, Wiley Online Library on [04/12/2024]. See the Terms and Conditions (https://onlinelibrary.wiley.com/terms-and-conditions) on Wiley Online Library for rules of use; OA articles are governed by the applicable Creative Commons License

Whiteley, J. S., Chambers, J. E., Uhlemann, S., Boyd, J. P., Cimpoiasu, M. O., Holmes, J. L., et al. (2020). Landslide monitoring using seismic refraction tomography – The importance of incorporating topographic variations. *Engineering Geology*, *268*, 105525. https://doi.org/10.1016/j.enggeo.2020.105525

Yang, K.-H., Uzuoka, R., Thuo, J. N., Lin, G.-L., & Nakai, Y. (2017). Coupled hydro-mechanical analysis of two unstable unsaturated slopes subject to rainfall infiltration. *Engineering Geology*, *216*(Supplement C), 13–30. https://doi.org/10.1016/j.enggeo.2016.11.006

Zreda, M., Shuttleworth, W. J., Zeng, X., Zweck, C., Desilets, D., Franz, T., & Rosolem, R. (2012). COSMOS: The cosmic-ray soil moisture observing system. *Hydrology and Earth System Sciences*, *16*(11), 4079–4099. https://doi.org/10.5194/hess-16-4079-2012

References From the Supporting Information

Rumble, J. (2018). *CRC handbook of chemistry and physics* (99th ed.). CRC Press.

19447973, 2024, 10, Downloaded from https://agupubs.onlinelibrary.wiley.com/doi/10.1029/2023WR036319 by British Geological Survey, Wiley Online Library on [04/12/2024]. See the Terms and Conditions (https://onlinelibrary.wiley.com/terms-and-conditions) on Wiley Online Library for rules of use; OA articles are governed by the applicable Creative Commons License